Water Resources Research

RESEARCH ARTICLE
10.1029/2019WR025528

Key Points:
- We present a model using concentration and isotope data to distinguish riparian denitrification from additional nitrate removal processes
- The model was applied to concentration and dual-element isotope data of nitrate from riparian groundwater wells
- Nitrate removal by additional processes greatly exceeded denitrification, particularly at larger distance from the river and in winter

Supporting Information:
- Supporting Information S1

Correspondence to:
S. R. Lutz,
stefanie.lutz@ufz.de

Citation:
Lutz, S. R., Trauth, N., Musolff, A., Van Breukelen, B. M., Knöller, K., & Fleckenstein, J. H. (2020). How important is denitrification in riparian zones? Combining end-member mixing and isotope modeling to quantify nitrate removal from riparian groundwater. *Water Resources Research*, *56*, e2019WR025528. https://doi.org/10.1029/2019WR025528

Received 8 MAY 2019
Accepted 4 DEC 2019
Accepted article online 11 DEC 2019

How Important is Denitrification in Riparian Zones? Combining End-Member Mixing and Isotope Modeling to Quantify Nitrate Removal from Riparian Groundwater

Stefanie R. Lutz[1], Nico Trauth[1], Andreas Musolff[1], Boris M. Van Breukelen[2], Kay Knöller[3], and Jan H. Fleckenstein[1]

[1]Department of Hydrogeology, Helmholtz Center for Environmental Research—UFZ, Leipzig, Germany, [2]Department of Water Management, Delft University of Technology, Delft, Netherlands, [3]Department of Catchment Hydrology, Helmholtz Center for Environmental Research—UFZ, Halle, Germany

Abstract Riparian zones are important buffer zones for streams as they are hotspots of nitrate transformation and removal in agricultural catchments. However, mixing of water from different sources and various transformation processes can complicate the quantification of nitrate turnover in riparian zones. In this study, we analyzed nitrate concentration and isotope data in riparian groundwater along a 2-km stream section in central Germany. We developed a mathematical model combining end-member mixing and isotope modeling to account for mixing of river water and groundwater and quantify nitrate transformation in riparian groundwater. This enabled us to explicitly determine the extent of denitrification (as process leading to permanent nitrate removal from riparian groundwater) and transient nitrate removal by additional processes associated with negligible isotope fractionation (e.g., plant uptake and microbial assimilation) and to perform an extensive uncertainty analysis. Based on the nitrogen isotope data of nitrate, the simulations suggest a mean removal of up to 27% by additional processes and only about 12% by denitrification. Nitrate removal from riparian groundwater by additional processes exceeded denitrification particularly in winter and at larger distance from the river, underlining the role of the river as organic carbon source. This highlights that nitrate consumption by additional processes predominates at the field site, implying that a substantial fraction of agricultural nitrogen input is not permanently removed but rather retained in the riparian zone. Overall, our model represents a useful tool to better compare nitrogen retention to permanent nitrogen removal in riparian zones at various temporal and spatial scales.

Plain Language Summary Nitrogen is an important nutrient for agricultural crops. However, excessive nitrogen input into surface water in the form of nitrate can lead to algae blooms and lack of oxygen. The riparian zones of rivers are important buffer zones where groundwater is connected to soils, which are rich in soil organisms and organic matter pools fueling reaction processes. Hence, plants and bacteria can remove nitrate from riparian groundwater before it reaches the river. Bacterial consumption of nitrate (denitrification) leads to complete removal of nitrogen via release of nitrogen gas into the atmosphere. In contrast, other biogeochemical processes such as nitrate uptake by plants merely result in nitrogen retention within riparian zones. To quantify the role of denitrification relative to other processes, we developed a novel model combining concentration and isotope data of nitrate and applied it to a groundwater study site in Central Germany. We found that nitrate removal from riparian groundwater by additional processes largely exceeded denitrification. Hence, a major fraction of nitrogen inputs was retained in the riparian zone and may eventually end up in the river. Such information is highly relevant for many river ecosystems at risk of eutrophication because of high nitrogen inputs from agriculture.

1. Introduction

Despite efforts to reduce nutrient inputs, the contamination of freshwater resources with nitrate (NO_3^-) poses a continuing problem in many European countries (European Union, 2010). For example, Germany has been taken to court by the European Commission due to insufficient measures to combat increasing

NO_3^- pollution of its freshwater resources (European Commission, 2016). Nitrogen (N) fertilizers and organic nitrogen in manure are major sources of nitrogen pollution, as crops assimilate part of the applied N only. The excessive N can be transformed to NO_3^- and leach to groundwater or enter rivers via direct runoff. In this context, riparian zones can act as buffers against NO_3^- pollution, as they are hydrologically and biogeochemically active zones where uptake and transformation of nutrients occur (Anderson et al., 2014; Dhondt et al., 2003; Hill, 1996; Mayer et al., 2007; Osborne & Kovacic, 1993; Vidon & Hill, 2004; Vought et al., 1994).

Nitrate removal from riparian groundwater can occur via various processes including denitrification of NO_3^- to N_2 or N_2O gas, plant uptake, microbial assimilation, dissimilatory NO_3^- reduction to ammonium (DNRA), and anaerobic ammonium oxidation (anammox) consuming nitrite (NO_2^-) derived from NO_3^- or NH_4^+ (Matheson et al., 2002; McPhillips et al., 2015; Naeher et al., 2015; Rivett et al., 2008). While all these processes reduce the risk of immediate NO_3^- pollution, denitrification is the only process that directly results in permanent N removal from riparian ecosystems via emission of N_2 and N_2O gas. In contrast, DNRA, microbial assimilation, and plant uptake lead to N retention in the riparian ecosystem, and anammox requires reduction from NO_3^- to NO_2^- by, for example, denitrifying bacteria before NO_2^- and ammonium (NH_4^+) are converted to N_2 (Burgin & Hamilton, 2007; Jahangir et al., 2017; Matheson et al., 2002). As the retained N might eventually be nitrified to NO_3^- and leach to riparian groundwater, the additional processes might result in transient NO_3^- removal only and are thus in contrast to permanent NO_3^- removal from riparian groundwater by denitrification. In order to accurately describe the fate of NO_3^- in riparian ecosystems, it is therefore vital to distinguish between denitrification and other biogeochemical processes acting on NO_3^- in riparian groundwater and to determine their relative contribution to overall (transient or permanent) removal of NO_3^- from riparian groundwater. Such information is, in turn, pertinent to the management of NO_3^- pollution in catchments, as understanding how, where and when denitrification efficiently removes NO_3^- from groundwater can support a targeted design of riparian buffer zones.

Quantification of denitrification rates is challenging as the end product of the transformation (i.e., N_2) is not easy to measure due to high background concentrations and spatial and temporal variability in denitrification rates (Groffman et al., 2006). The magnitude of in situ denitrification in riparian zones has typically been assessed using the acetylene block method (Bragan et al., 1997; Clément et al., 2003; McCarty et al., 2007), ^{15}N-labelled NO_3^- in "push-pull" experiments (Anderson et al., 2014; McPhillips et al., 2015), the N_2:Ar method (Blicher-Mathiesen et al., 1998; Böhlke et al., 2002), and NO_3^- concentration gradients in conjunction with chloride as a conservative natural tracer to account for dilution (Hill et al., 2014; Schilling et al., 2017; Trauth et al., 2018). However, field-scale quantification of denitrification in riparian groundwater remains challenging (Rivett et al., 2008) as these methods work at a local scale and can become impractical and expensive under in situ conditions (Groffman et al., 2006). Moreover, denitrification rates are controlled by local factors including NO_3^- and oxygen concentrations, temperature, and availability of electron donors such as organic carbon (Anderson et al., 2014; Burgin & Hamilton, 2007; Rivett et al., 2008). These factors can vary substantially both in time and space such that a limited number of in situ experiments might fail to accurately describe seasonal and spatial variations of denitrification in riparian groundwater.

Previous field studies distinguishing denitrification from other NO_3^- removal processes in riparian groundwater have mostly employed isotopically labelled NO_3^-. They have reported significantly differing contributions of denitrification to overall NO_3^- removal, depending on the analyzed system and field conditions. For example, using push-pull experiments in a riparian aquifer next to a third-order stream in central New York, McPhillips et al. (2015) attributed 5%–12% of total NO_3^- consumption to riparian denitrification and a similar contribution to DNRA, in contrast to 29%–69% that might have been removed by plant uptake, abiotic immobilization, and microbial assimilation. Using the same method, Jahangir et al. (2017) assessed removal contributions of around 15% by denitrification and 40%–63% by DNRA in groundwater beneath constructed wetlands in southeastern Ireland. These somewhat deviating results highlight the need for more research into methods quantifying denitrification relative to other processes in freshwater systems (Burgin & Hamilton, 2007; McPhillips et al., 2015). Considering the spatial and temporal limitations of experiments with isotopically labelled NO_3^-, analyzing field isotope data of NO_3^- might be a viable alternative tool for quantification of NO_3^- removal from riparian groundwater over longer periods and under varying field conditions.

Removal processes of NO_3^- occurring in riparian groundwater can entail changes in the isotopic composition of the residual NO_3^- (i.e., kinetic isotope fractionation). Among all removal processes, denitrification entails the most significant isotope fractionation effects in both nitrogen and oxygen (N and O) isotopes, whereas other removal processes occurring in riparian zones such as plant uptake or assimilation by cyanobacteria are usually associated with considerably smaller or no isotope fractionation effects (Bauersachs et al., 2009; Dhondt et al., 2003; Granger et al., 2008; Kendall, 1998; Mariotti et al., 1982; Yoneyama et al., 2001). Hence, changes in the environmental isotopic composition of NO_3^- have been used as qualitative evidence for denitrification in groundwater (Clément et al., 2003; Mengis et al., 1999; Wexler et al., 2014). However, the environmental isotopic composition of NO_3^- has been rarely used to quantify the extent of denitrification in riparian zones. One exception is a study conducted in the riparian zone of a second-order river in Belgium (Dhondt et al., 2003), which reports seasonally varying contributions of denitrification (between 49% and 75%) and plant uptake (between 25% and 51%) to overall NO_3^- removal under the assumption of limited isotope fractionation for plant uptake compared to denitrification. However, this approach did not account for reduction in NO_3^- concentrations due to mixing or transformation processes additional to plant uptake, which might distort the estimates of denitrification and plant uptake under typical field conditions in riparian zones (i.e., mixing of groundwater and river water and simultaneous occurrence of different biogeochemical processes).

The combined analysis of N and O isotopes of NO_3^- (i.e., the dual-isotope approach) has proven beneficial for deciphering NO_3^- sources and distinguishing between isotopic changes due to denitrification versus mixing of several sources (Kendall, 1998; Xue et al., 2009). Dual-isotope mixing models for NO_3^- have been applied to distinguish major natural and anthropogenic NO_3^- sources in rivers and groundwater, mostly by assuming negligible denitrification or including denitrification in uncertainty terms (Deutsch et al., 2006; Kim et al., 2015; Matiatos, 2016; Wang et al., 2016). However, there is a lack of methods utilizing the strength of the dual-isotope approach to distinguish changes in the isotopic composition of NO_3^- caused by denitrification from those caused by mixing (e.g., between groundwater and river water), which is needed to accurately quantify denitrification in riparian zones.

In view of the importance of denitrification for reducing NO_3^- inputs to freshwater, the general potential of isotopic methods as well as their limitations in denitrification quantification, the aim of this study was to develop and test a model able to quantify both denitrification and additional removal processes in riparian zones in the presence of two mixing NO_3^- sources. We summarize under the term additional processes all uptake and transformation processes other than denitrification that lead to NO_3^- removal from riparian groundwater and subsequent N retention in the riparian zone. To distinguish between denitrification, additional removal processes and dilution due to mixing, we adapted the recently developed stable isotope sources and sinks (SISS) model (Lutz & Van Breukelen, 2014a) to concentration and dual-element isotope data of NO_3^- from riparian groundwater and combined this model with a conventional chloride mixing model providing the extent of overall NO_3^- removal from riparian groundwater. The SISS model allows for quantification of both transformation and mixing between two sources using compound-specific isotope data. While the model has been previously applied to a locally polluted aquifer (Lutz & Van Breukelen, 2014b), this study represents the first application of the SISS model to a diffuse pollutant such as agricultural NO_3^-, which can be subject to a variety of biogeochemical processes in riparian zones additional to dilution and permanent removal and thus requires the extension of the original SISS model. In the following, we illustrate the derivation and application of the modified SISS model (SISS-N) using the example of a groundwater study area along a 2-km stream section in central Germany.

2. Field Site and Data

2.1. Field Site Description

We examined a 2-km stretch along the Selke River in Central Germany (Figure 1) located in the Harz/Central German Lowland Observatory of the TERrestrial ENviromental Observatories network (Wollschläger et al., 2016; Zacharias et al., 2011). The Selke Catchment has a total size of 456 km^2, of which 200 km^2 are upstream of the field site. The catchment can be broadly divided into the more forested upstream part in the Harz Mountains and the agricultural downstream part in the lowland area (Figure 1a). Fertilizer application on agricultural fields is the main N source in the catchment (Rode et al., 2016). Previous studies

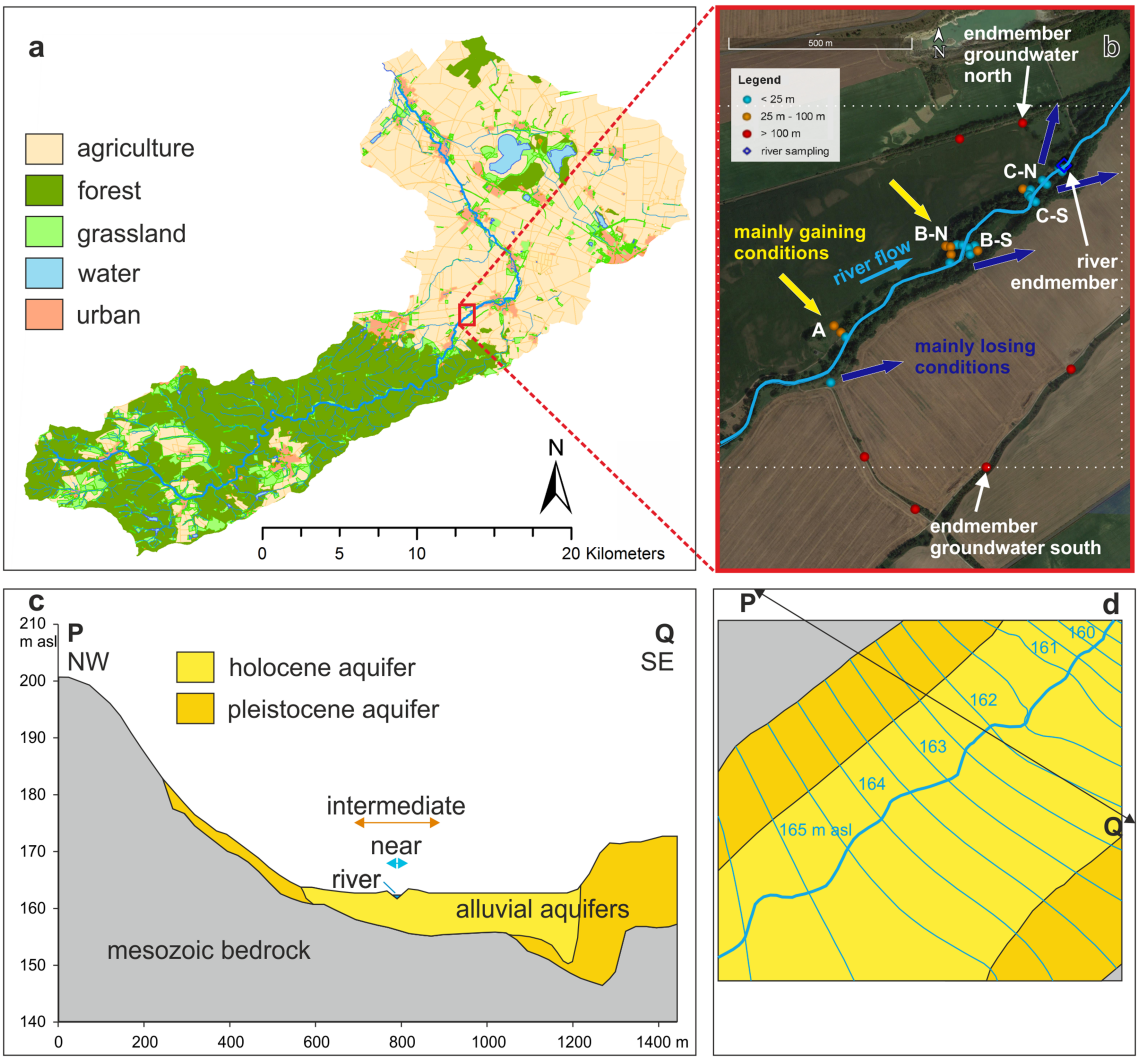

Figure 1. Land use in the Selke Catchment and location of the field site (a); overview of the field site (b) with distant groundwater wells (red dots, distance of >100 m from the river), groundwater wells in the riparian zone (blue dots, distance of <25 m from the river, and orange dots, distance of 25–55 m from the river) and river sampling point (dark blue diamond); schematic cross section of the field site indicating hydrogeological setup and location of the riparian zone (c); and plan view of the field site delimited by the dotted rectangle in (b) with interpolated groundwater levels in blue (m a.s.l.) (d). The location of the cross section in (c) is indicated in (d) by the line from P to Q. Letters A–C in (b) represent different well transects, with N and S indicating the location north and south of the Selke River, respectively.

in the field site area have analyzed hyporheic exchange (Trauth et al., 2015; Trauth & Fleckenstein, 2017), hydrochemical gradients between the unsaturated zone and groundwater (Gassen et al., 2017), riparian travel times (Nixdorf & Trauth, 2018), and NO_3^- removal in the riparian zone (Trauth et al., 2018).

The field site has been extensively described in Trauth et al. (2018). In brief, annual mean air temperature was 8.8 °C and monthly mean air temperatures ranged from 0.4 °C in January to 18.0 °C in July between 1981 and 2010 (average of three meteorological stations at a distance of below 15 km from the field site; Deutscher Wetterdienst (DWD) Climate Data Center, 2018). Mean annual rainfall was 582 mm and mean monthly rainfall ranged from 36 mm in February to 63 mm in July between 1981 and 2010 (average of four stations at a distance of <15 km; DWD Climate Data Center, 2018). The Selke River at the field site meanders and flows through distinct pool-riffle sequences including in-stream gravel bars with an annual mean discharge of 1.5 $m^3 s^{-1}$. It is buffered from the surrounding agricultural fields by riparian vegetation (mainly willow, beech, and pasture) with a maximum width of 50 m at both sides. Groundwater generally flows parallel to the river toward the northeast, while mixing between groundwater and river water occurs in the

proximity of the Selke River due to the meandering river channel depending on hydrologic conditions and channel morphology (Nixdorf & Trauth, 2018). Chloride concentrations in riparian groundwater and the river suggest that the A and B-N transects are less impacted by infiltrating river water compared to the other well clusters (Figure 1b; Trauth et al., 2018). The aquifer is mainly composed of alluvial sand and gravel deposits transported by the river from the Harz Mountains to the alluvial plains. At the field site, the aquifer has a maximum thickness of 8 , is covered by up to 1.2 m of alluvial loam, and overlies an aquitard consisting of silty clay. Hydraulic conductivity in the aquifer of the riparian zone determined from salt tracer tests ranges from 1.7×10^{-3} to 1.2×10^{-2} m s^{-1}. Depth to groundwater in the riparian zone ranges from 2 m during summer to 0.5 m during winter.

2.2. Monitoring Setup, Hydrochemical, and Isotopic Analyses

Groundwater was monitored in 30 wells (inner diameter of 2.54 to 5.05 cm), among which 24 were located within the riparian zone (Figure 1b). The length of the well screens ranged between 1 and 3 m, giving a maximum screening depth of 4- to 5-m below ground in the wells close to the river and up to 8-m below ground in the more distant wells. The groundwater wells were classified according to their distance from the Selke River into a near groundwater (distance of <25 m), intermediate groundwater (distance of 25–55 m) and distant groundwater zone (distance of >100 m). The wells in the riparian zone were all assigned to the near or intermediate groundwater zones. Moreover, river water was sampled close to the most downstream riparian wells (Figure 1b).

Monthly time series for hydrochemical and NO_3^- isotope data for the well and river samples were taken from Trauth et al. (2018), including dissolved oxygen, cations (Ca^{2+}, Fe^{2+}, K^+, Mg^{2+}, Na^+, and NH_4^+), anions (Cl^-, NO_3^-, NO_2^-, PO_4^{3-}, SO_4^{2-}), dissolved organic carbon (DOC), alkalinity (HCO_3^-), redox potential (E_h), electrical conductivity (EC), pH, temperature, groundwater level as well as N and O isotope data of NO_3^-, and hydrogen and oxygen isotope data of water. Moreover, discharge at the river sampling point was measured on the same sampling dates. Sampling mostly occurred during average to low-flow conditions in the river. Detailed information on analytical methods and their uncertainties can be found in Trauth et al. (2018).

Nitrate isotope analyses were performed using a GasBench II connected to an Isotope Ratio Mass Spectrometer (DELTA V plus; Thermo Scientific) following conversion of NO_3^- to N_2O using the bacterial denitrifier method (Casciotti et al., 2002; Sigman et al., 2001). The isotope values express the relative abundance of heavy versus light isotopes of N and O, respectively (i.e., the isotope ratio); they are reported in per mille as $\delta^{15}N$ and $\delta^{18}O$ values with respect to the international standards of atmospheric N (isotope ratio of AIR $N_2 = 3.667 \times 10^{-3}$) for N and Vienna standard mean ocean water (isotope ratio of VSMOW $= 2.0052 \times 10^{-3}$) for O:

$$\delta_S = \frac{IR_S}{IR_{ref}} - 1 \quad (1)$$

where δ_S is the isotope value of the sample (i.e., $\delta^{15}N$ or $\delta^{18}O$), IR_S is the isotope ratio of the sample, and IR_{ref} is the isotope ratio of the international reference (i.e., AIR N_2 or VSMOW). The analytical uncertainties of the isotope analyses in this study were ±0.4‰ for $\delta^{15}N$ and ±1.6‰ for $\delta^{18}O$. In addition, stable water isotope values (i.e., δ^2H-H_2O relative to VSMOW $= 1.5576 \times 10^{-4}$ and $\delta^{18}O$-H_2O relative to VSMOW $= 2.0052 \times 10^{-3}$) were determined for riparian groundwater and river samples as well as for rainfall close to the field site using cavity ring-down spectroscopy (L2130-i, Picarro Inc.) with analytical uncertainties of 1.0‰ for δ^2H-H_2O and 0.3‰ for $\delta^{18}O$-H_2O.

2.3. Hydrochemical Characterization

In the following, we briefly present the chloride (Cl^-) concentrations, NO_3^- concentrations and NO_3^- isotope data, which are required for the application of the SISS-N model. We consider the river sampling point close to the well transect C (Figure 1b) as river end-member. For the groundwater end-member, we chose two different wells in the distant groundwater as separate end-members for the southern and the northern part of the field site (Figure 1b), as the agricultural fields in the north of the river differ from the fields in the south in terms of area, agricultural practices and groundwater NO_3^- concentrations (Figure 2c). This agrees

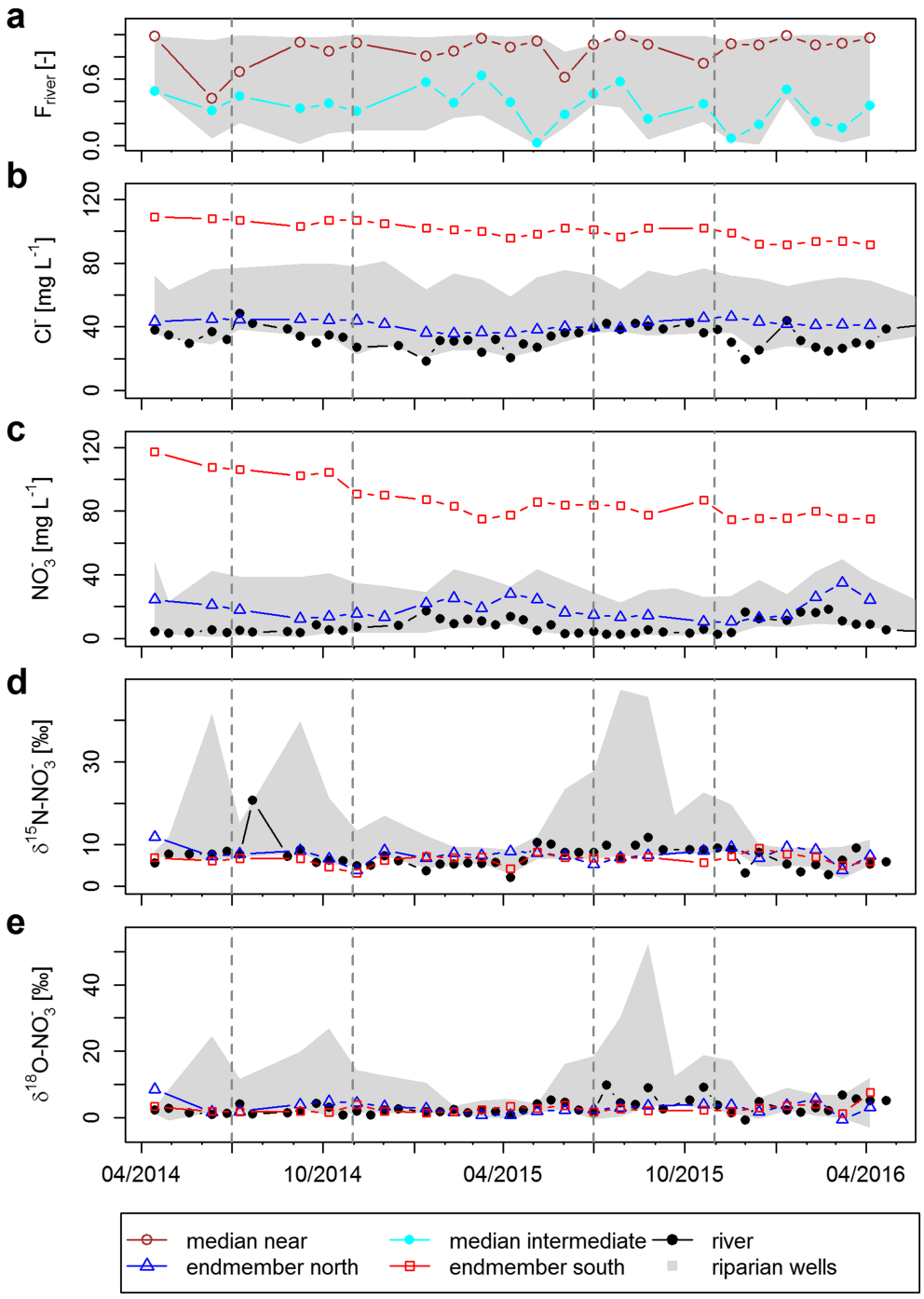

Figure 2. River water fraction (F_{river}, a) in the near groundwater (brown dots), intermediate groundwater (cyan dots) and all riparian wells (grey area); and chloride concentrations (b), NO_3^- concentrations (c), and NO_3^- isotope values (d and e) of the river end-member (black dots), northern groundwater end-member (blue triangles), southern groundwater end-member (red squares) and all riparian wells (grey area). The period from July to November is indicated by vertical dashed lines.

with the assumptions in Trauth et al. (2018) for the calculation of the fraction of river water in the riparian groundwater samples (F_{river}, scaling from 0 to 1) and total NO_3^- removal. Trauth et al. (2018) assessed F_{river} using an end-member mixing model with Cl^- concentrations (equation (2) below). They computed larger mean F_{river} values in the near than in the intermediate groundwater (mean of 0.8 ± 0.24 vs. 0.34 ± 0.23; Figure 2a and Table S1 in the supporting information).

Mean Cl^- concentrations in the distant groundwater were twice as high as river concentrations (67.2 ± 24.4 and 33.2 ± 6.7 mg L^{-1}, respectively), with the intermediate and near groundwater concentrations (49.1 ± 13.5 and 35.7 ± 9.0 mg L^{-1}, respectively) lying in between (Table S1). For the southern groundwater end-member, Cl^- concentrations show a slightly decreasing trend (Figure 2b) from 109.0 to 91.7 mg L^{-1} over the study period, while there was no obvious temporal trend for the northern groundwater end-member. Chloride concentrations of the river end-member ranged between 18.6 and 48.4 mg L^{-1} and were mostly below Cl^- concentrations in riparian groundwater (Figure 2b).

Similar to Cl^- concentrations, mean NO_3^- concentrations in the distant groundwater (65.3 ± 36.5 mg L^{-1}) exceeded by far those in the intermediate groundwater (15.5 ± 10.4 mg L^{-1}), near groundwater (8.5 ± 4.9 mg L^{-1}), and river (7.6 ± 4.6 mg L^{-1}; Table S1). Nitrate concentrations of the northern groundwater end-member (Figure 2c) show no clear trend during the study period. In contrast, concentrations of the southern groundwater end-member decreased from high concentrations of up to 117.2 to 75.1 mg L^{-1} at the end of the study period, possibly as a result of decreasing fertilizer application and thus N surplus from agriculture in the region (Bach & Frede, 1998). Nitrate concentrations in riparian groundwater (Figure 2c) generally exceeded those in the river, peaked in spring, and decreased in summer.

Mean $\delta^{15}N$ values were lowest in the river (7.2‰ ± 2.9‰) and highest in the near groundwater (9.9‰ ± 6.8‰), with the values of the intermediate (8.3‰ ± 3.4‰) and distant groundwater (7.6‰ ± 2‰) lying in between (Table S1). River $\delta^{15}N$ values ranged between 2.2‰ and 20.8‰ over the study period (Figure 2d). The $\delta^{15}N$ values at the river sampling point were similar to those measured 1.5-km upstream in the Selke River and in a small tributary discharging into the Selke River just upstream of the field site (data not shown). Moreover, the $\delta^{15}N$ values of the two groundwater end-members covered a smaller range than those of the river (Figure 2d), while the $\delta^{15}N$ values in the riparian zone largely exceeded the end-member signatures.

In line with the $\delta^{15}N$ values, the $\delta^{18}O$ values of NO_3^- where higher in the near and intermediate groundwater (means of 6.2‰ ± 6.5‰ and 4.0‰ ± 3.6‰, respectively; Table S1) compared to the distant groundwater and the river (means of 3.0‰ ± 1.9‰ and 3.1‰ ± 2.3‰, respectively). The temporal dynamics of $\delta^{18}O$ values were generally similar to the dynamics of $\delta^{15}N$ values, with a large enrichment (i.e., increase in isotope values) in the riparian zone compared to the river and the two groundwater end-members (Figure 2e). The location of the riparian groundwater samples in the dual-isotope space points toward soil N, manure, and sewage as main NO_3^- sources and shows considerable isotopic enrichment in both $\delta^{15}N$ and $\delta^{18}O$ outside of the typical source ranges for some samples (Trauth et al., 2018).

3. Mixing and Transformation Models

3.1. Model Assumptions

We combined two different models in the assessment of mixing between river water and groundwater and NO_3^- removal: a linear mixing model using Cl^- and NO_3^- concentrations and the SISS model (Lutz & Van Breukelen, 2014a) using the $\delta^{15}N$ and $\delta^{18}O$ values of NO_3^-. The modified SISS model (SISS-N; derived below) provided the extent of denitrification, whereas the linear mixing model was used to calculate the fraction of river water in each sample (F_{river}) from Cl^- concentrations and, subsequently, derive total NO_3^- removal from riparian groundwater using F_{river} and NO_3^- concentrations. In the original SISS model, Cl^- and NO_3^- concentrations would not be needed, as the end-member contributions (here, F_{river}) would be calculated from the dual-element isotope data alone. In the SISS-N model, however, we used the end-member contributions from the Cl^- mixing model to allow a direct comparison between overall NO_3^- removal (known from the Cl^- mixing model) and extent of denitrification. Moreover, unlike the dual-element isotope data, Cl^- concentrations generally differ between the distant groundwater and the river, which permits a clear distinction between the two end-members (Figure 2b; see also section 3.3).

For simplicity and as temporal changes in groundwater flow paths are not known, we considered each sampling date separately and assumed that (i) the isotope signatures of the wells in the riparian zone result from mixing between the two end-members (i.e., river end-member and northern or southern groundwater end-member) and (ii) mixing occurs prior to any significant removal processes in the riparian zone. We restricted the model to the two end-members as we consider lateral flow in shallow soil and associated Cl^- and NO_3^-

fluxes as secondary due to the fact that samples were mostly taken during average to low-flow conditions and because the aquifer at the field site is highly conductive, as opposed to the overlying loamy sediments. This model assumption thus agrees with the finding that riparian groundwater at the field site is mainly governed by infiltrating river water at shallow depths and by regional groundwater at greater depth (Gassen et al., 2017). Regarding assumption (ii), we postulate that the end-member signatures are not subject to significant isotope fractionation before mixing, in agreement with end-member mixing models that assume conservative end-member concentrations. This yields a conservative (i.e., smaller) estimate of the extent of denitrification with the SISS-N model in comparison to scenarios of prior denitrification before mixing (Lutz & Van Breukelen, 2014a).

We assumed that denitrification is the only process occurring at the field site that entails significant isotope fractionation in both N and O isotopes. Isotope fractionation effects during other NO_3^- removal processes in groundwater and riparian zones are generally unknown (e.g., DNRA; Nikolenko et al., 2018) and, when reported, refer only to the nitrogen isotopic composition of NO_3^-. There is evidence of limited isotope fractionation in nitrogen isotopes during plant uptake (Dhondt et al., 2003; Mariotti et al., 1982), and most studies have associated plant uptake with negligible isotope fractionation compared to denitrification (Högberg et al., 1999; Lund et al., 1999). Moreover, we do not distinguish between heterotrophic and autotrophic denitrification (i.e., oxidation of organic carbon vs. inorganic compounds), as the extent of isotope fractionation associated with autotrophic denitrification is assumed similar to that of heterotrophic denitrification (Torrentó et al., 2010; Torrentó et al., 2011).

The SISS-N model only considers isotope fractionation in NO_3^- isotopes. Hence, it does not indicate whether N_2 has been produced by denitrifying or anammox bacteria, as the first reaction step of both complete denitrification and anammox is the conversion of NO_3^- to NO_2^- by denitrifying bacteria. It follows that the SISS-N model assessment of NO_3^- removal from groundwater is not affected by the potential occurrence of anammox, unless there is a significant fraction of NO_2^- in riparian groundwater that is produced by other processes than denitrification and subsequently reduced to N_2 by anammox bacteria. The latter is not likely for our field site, as riparian groundwater is highly influenced by infiltration of river water, which does not favor the slowly growing anammox bacteria requiring stable conditions with little water exchange rates (Wang et al., 2020). Similarly, river water infiltration provides organic carbon to riparian groundwater, whereas anammox is assumed to occur primarily when organic carbon supply is low (e.g., Burgin & Hamilton, 2007; Du et al., 2019). Third, the low NO_2^- and NH_4^+ concentrations do not suggest a substantial role of anammox at our field site. Hence, while we cannot fully rule out the occurrence of anammox at the field site, we will focus on the comparison between denitrification and additional nonfractionating processes in the following.

3.2. River Water Fractions and Total Nitrate Removal

Chloride was considered as conservative tracer for the mixing processes between distant groundwater and river water that result in mixed samples in the riparian groundwater wells. The fraction of river water in these samples was determined as

$$F_{river} = \frac{[Cl^-_{rip}] - [Cl^-_{dist}]}{[Cl^-_{river}] - [Cl^-_{dist}]} \quad (2)$$

where $[Cl^-_{rip}]$, $[Cl^-_{dist}]$, and $[Cl^-_{river}]$ denote the chloride concentrations of the riparian groundwater sample, distant groundwater end-member, and river water end-member, respectively, on each sampling day. The F_{river} values in this study deviate from those in Trauth et al. (2018) due to the incorporation of analytical uncertainties in the model (see section 3.5).

Knowing F_{river} allows calculation of the theoretical NO_3^- concentration in the riparian groundwater sample that would occur under the same mixing conditions between distant groundwater and river water in the absence of any NO_3^- removal processes:

$$[NO_3^- mix] = \left([NO_3^- river] - [NO_3^- dist]\right) \times F_{river} + [NO_3^- dist] \quad (3)$$

where $[NO_3^-_{mix}]$ is the theoretical concentration following mixing in riparian groundwater and $[NO_3^-_{river}]$ and $[NO_3^-_{dist}]$ are the NO_3^- concentrations of the river and groundwater end-member, respectively.

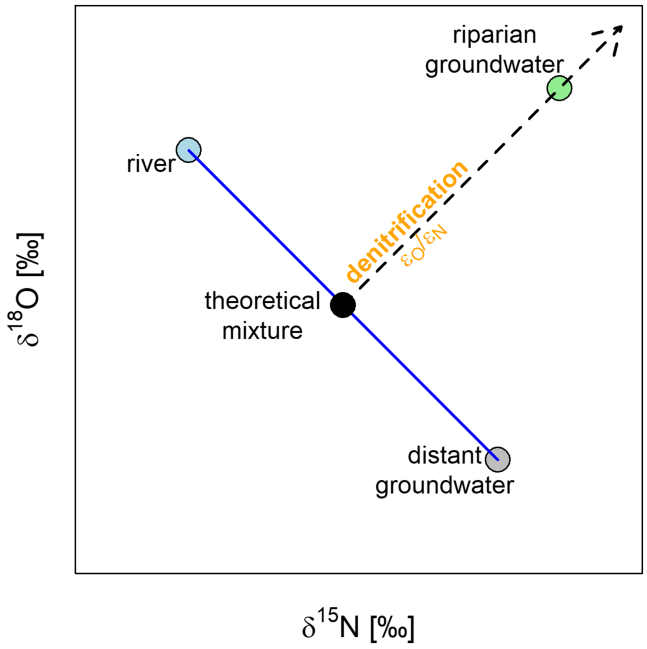

Figure 3. Illustration of the SISS-N model in the dual-isotope space assuming mixing between the end-members of distant groundwater and river water with subsequent denitrification. The solid blue line represents the mixing line between the end-members, and the dashed black line shows the denitrification trajectory with a slope approximately equal to the ratio between the enrichment factors ε_O and ε_N.

Comparing $[NO_3^-{}_{mix}]$ to the actual NO_3^- concentration of the riparian groundwater sample $[NO_3^-{}_{rip}]$ yields the total extent of removal from groundwater:

$$R_{tot}[\%] = \frac{[NO_3^- mix] - [NO_3^- rip]}{[NO_3^- mix]} \times 100\% \quad (4)$$

where R_{tot} (in %) describes the net NO_3^- removal from riparian groundwater comprising NO_3^- production and removal processes (e.g., nitrification, denitrification, and assimilation into biomass).

Equation (2) can only be applied if $[Cl^-{}_{rip}]$ lies within the range delimited by the end-member concentrations $[Cl^-{}_{dist}]$ and $[Cl^-{}_{river}]$. Similarly, equation (4) is valid only for samples with $[NO_3^-{}_{mix}] \geq [NO_3^-{}_{rip}]$.

3.3. Denitrification and Additional Fractionating Processes

Denitrification and additional fractionating processes were assessed with a modified version of the SISS model, which has been developed to quantify mixing and degradation of a pollutant in a scenario of two mixing sources and degradation using compound-specific isotope data. Lutz and Van Breukelen (2014a) provided a detailed derivation and description of the SISS model. In brief, while simultaneous occurrence of mixing and degradation processes complicates the use of isotope mixing models, the SISS model disentangles the effects of these processes on the isotope data and thus allows quantification of both mixing and degradation.

For this study, the original SISS model was modified by using the river water fractions (F_{river}) calculated with equation (2) to determine the theoretical isotope value of the riparian groundwater sample following mixing between river water and groundwater in the absence of denitrification:

$$\delta^{15}N_{mix} = F_{river} \times \delta^{15}N_{river} + (1 - F_{river}) \times \delta^{15}N_{dist} \quad (5)$$

$$\delta^{18}O_{mix} = F_{river} \times \delta^{18}O_{river} + (1 - F_{river}) \times \delta^{18}O_{dist} \quad (6)$$

where $\delta^{15}N$ and $\delta^{18}O$ are the N and O isotope values of NO_3^- for the river water end-member (subscript *river*), distant groundwater end-member (subscript *dist*), and riparian groundwater sample (subscript *mix*). The mixing signature ($\delta^{15}N_{mix}$, $\delta^{18}O_{mix}$) lies on the mixing line between the end-member signatures of the river ($\delta^{15}N_{river}$, $\delta^{18}O_{river}$) and distant groundwater ($\delta^{15}N_{dist}$, $\delta^{18}O_{dist}$) in the dual-isotope space (Figure 3). In the original version of the SISS model, the mixing signature is determined in the dual-isotope space by the intersection between the mixing line and the degradation trajectory, which describes the increase in isotope values of both isotopic elements with ongoing degradation (i.e., black dashed line in Figure 3). For the SISS-N model, we calculated the mixing signature using F_{river} instead to be consistent in the computation of total NO_3^- removal (equation (4)) and extent of denitrification and thus allow a direct comparison between the two. This also avoids large uncertainties in F_{river} with the original SISS model resulting from similar dual-element isotope signatures of the two end-members on some sampling dates (Text S1 and Figure S1). This might especially occur if NO_3^- primarily originates from one source, as is the case at the field site given the predominance of agricultural NO_3^-. While it is generally possible to derive F_{river} from $\delta^{15}N\text{-}NO_3^-$ and $\delta^{18}O\text{-}NO_3^-$ data, we computed F_{river} in this study from the generally distinct Cl^- end-member concentrations and used the two isotopic elements instead to obtain two independent model results for the extent of denitrification.

The change in the isotope ratio (i.e., isotope fractionation) associated with denitrification can be described using the Rayleigh equation (Mariotti et al., 1981):

$$\frac{IR_t}{IR_0} = f_{den}^{(\alpha-1)} \tag{7}$$

where IR_0 and IR_t are the isotope ratios of NO_3^- at time 0 and time t, respectively, f_{den} is the nondenitrified fraction of NO_3^- at time t, and α is the isotope fractionation factor describing the strength of isotope fractionation during denitrification. The α value is typically expressed in per mille as isotopic enrichment factor $\varepsilon = (\alpha - 1)$ (Coplen, 2011). In the dual-element isotope plot, the ratio of the two enrichment factors (e.g., $\varepsilon_O/\varepsilon_N$) is approximately equal to the slope of the degradation trajectory (Figure 3).

According to equations (1) and (7), the remaining NO_3^- fraction in the riparian groundwater sample after denitrification of the theoretical mixture is given by

$$f_{den} = \left(\delta\frac{^{15}N_{rip} + 1000}{\delta^{15}N_{mix} + 1000}\right)^{\frac{1000}{\varepsilon_N}} \tag{8}$$

where $\delta^{15}N_{mix}$ and $\delta^{15}N_{rip}$ are the nitrogen isotope values of the theoretical mixture and riparian groundwater sample, respectively, and ε_N is the enrichment factor assumed representative of denitrification-induced isotope fractionation. Equation (8) was analogously applied using the O isotope values ($\delta^{18}O_{mix}$ and $\delta^{18}O_{rip}$) and enrichment factor (ε_O) to allow for comparison with the results using $\delta^{15}N$ and ε_N. As we assumed that denitrification is the only NO_3^- removal process associated with significant isotope fractionation at the field site, the dual-element isotope data were not used to distinguish between different transformation pathways, unlike in Lutz and Van Breukelen (2014b).

Quantification of removal by denitrification follows from equation (8):

$$R_{den}[\%] = (1 - f_{den}) \times 100\% \tag{9}$$

Nitrate removal by processes other than denitrification (R_{add}) can be determined as the difference between total removal (R_{tot}, equation (4)) and removal by denitrification (R_{den}, equation (9)):

$$R_{add}[\%] = R_{tot} - R_{den} \tag{10}$$

R_{den} and R_{add} were calculated analogously using O isotope data and ε_O. Negative R_{add} values (i.e., $R_{den} > R_{tot}$) were set to zero unless mentioned otherwise.

The percentages given by equations (4), (9), and (10) are not to be understood as relative contributions to overall NO_3^- removal but as removal percentages relative to the theoretical NO_3^- concentration that would occur without any transformation or retention processes.

3.4. Specification of Isotopic Enrichment Factors

According to equation (8), NO_3^- concentrations and isotope values before and after denitrification at our field site are related via the apparent isotopic enrichment factor ε_{app}:

$$\Delta = 1,000 ln\left(\frac{\delta_{rip} + 1}{\delta_{mix} + 1}\right) = ln(f_{den}) \times \varepsilon_{app} = ln\left(\frac{[NO_3^- rip]}{[NO_3^- mix]}\right) \times \varepsilon_{app} \tag{11}$$

where Δ is the isotopic shift, $[NO_3^-{}_{mix}]$ is the theoretical NO_3^- concentration of the mixture (equation (3)), $[NO_3^-{}_{rip}]$ is the actual NO_3^- concentration in riparian groundwater, δ_{mix} is the theoretical isotope value (i.e., $\delta^{15}N_{mix}$ or $\delta^{18}O_{mix}$) of the mixture known from equations (5) to (6), and δ_{rip} is the isotope value measured in riparian groundwater. Equation (11) thus accounts for concentration decreases due to dilution and, when applied to field data, incorporates the combined effect of fractionating (i.e., denitrification) and nonfractionating processes (i.e., additional processes) on NO_3^- isotope values via ε_{app}.

Provided the presence of additional NO_3^- removal processes at our field site, isotopic enrichment factors derived from our field data are bulk ε-values resulting from denitrification-induced isotope fractionation

and decreasing concentrations due to additional nonfractionating processes. Hence, they are likely to be smaller in absolute terms (i.e., less negative) than laboratory-derived enrichment factors using isolated bacterial cultures (Dhondt et al., 2003; Knöller et al., 2011). In order to delimit ε values representative of pure denitrification at the field site, we calculated the apparent enrichment factors for N and O (i.e., $\varepsilon_{N,app}$ and $\varepsilon_{O,app}$) for each season using equation (11) and compared them to laboratory-derived values of ε_N and ε_O from literature (see section 4.1). Given the impact of additional removal processes on apparent isotope fractionation measured in the field, we refrained from a direct use of the field-derived $\varepsilon_{N,app}$ and $\varepsilon_{O,app}$ values in the calculation of R_{den}. Instead, we assumed that apparent enrichment factors close to laboratory-derived values are representative of denitrification-induced isotope fractionation occurring at the field site under conditions of little interference by additional removal processes.

3.5. Uncertainty Calculations

In order to include the analytical uncertainties of concentration and isotope data, we conducted 10,000 Monte Carlo simulations of the SISS-N model, assuming the concentrations and isotope values of the end-members and riparian groundwater samples ($n = 482$) to be normally distributed around their measured values with the following standard deviations: 3% for Cl^- (equation (2)) and NO_3^- (equations (3) and (4)) concentrations (i.e., maximum measurement error of ion-chromatography), 0.4‰ for $\delta^{15}N$ and 1.6‰ for $\delta^{18}O$ (i.e., standard errors of the isotope analyses; equations (5), ((6), (8), and (11)). This yielded valid SISS-N model results (either for SISS-N with N isotope data and SISS-N with O isotope data or both) for substantially more samples ($n = 337$) than without consideration of analytical uncertainties in concentration and isotope data ($n = 183$). The SISS-N model results for a riparian groundwater sample were considered valid if $0 \leq F_{river} \leq 1$ (equation (2)) and $0 \leq f_{den} \leq 1$ (equation (8)) in at least 100 Monte Carlo simulations (i.e., 1% of all simulations). Increasing this threshold to 10% of all simulations had little effect on the SISS-N model results (not shown). Analytical uncertainties in concentration and isotope data were incorporated accordingly into equation (11) to account for their impact on apparent isotopic enrichment factors. Uncertainties in R_{den} and R_{add} associated with the choice of ε_N and ε_O are discussed in section 5.3.

In addition to considering analytical uncertainties, we also analyzed how our results were affected by the assumption of instantaneous mixing prior to denitrification (i.e., the base scenario). Given the proximity of the riparian groundwater wells to the river, this assumption seems less critical for the river end-member compared to the distant groundwater end-members: The northern and southern end-members are located at distances of 167 and 503 m, respectively, from the river and might thus undergo significant denitrification before mixing with the river water in the riparian zone. To assess the effect of prior denitrification of the groundwater end-members, we determined the total extent of denitrification ($R_{den,ext}$; equation (S1)) of the riparian groundwater sample in an extreme scenario assuming maximum denitrification before mixing for the groundwater end-members and no denitrification before mixing for the river end-member. This scenario implies that denitrification occurs prior to mixing and in groundwater only and that any removal following mixing between groundwater and river water occurs via additional processes. To simulate this, we set R_{den} of the river end-member to zero and R_{den} of the respective groundwater end-member to the maximum value possible considering F_{river} and the mixing line between the source signature of the river end-member and the riparian groundwater sample (Figure S2). It follows that $R_{den,ext}$ is defined solely by F_{river} and the isotope value of the groundwater end-member undergoing maximum denitrification (equation (S1)). We calculated the deviation of R_{den} and R_{add} in the extreme scenario from the base-scenario values (i.e., $R_{den,ext}$ vs. R_{den} and $R_{add,ext}$ vs. R_{add}, respectively) in 10,000 Monte Carlo simulations, using the same probability distributions for the concentration and isotope values of end-members and riparian groundwater as in the base scenario. We considered only those simulations with $0 \leq R_{den} \leq 100\%$ and $0 \leq R_{den,ext} \leq 100\%$. Moreover, as in the base scenario, we set all negative $R_{add,ext}$ values to zero. As the end-member contributions are set to F_{river} and not derived from the dual-element isotope data, $R_{den,ext}$ using $\delta^{15}N$ and ε_N differs from $R_{den,ext}$ using $\delta^{18}O$ and ε_O.

Further model uncertainties might be associated with evaporation effects in the riparian zone that increase Cl^- and NO_3^- concentrations (i.e., evapoconcentration; Ong et al., 1995) of riparian groundwater samples and thus affect the Cl^- mixing model (equations (2)–((4)). While the concentration increase associated with evapoconcentration is difficult to quantify, we assessed its impact on the SISS-N model results indirectly by

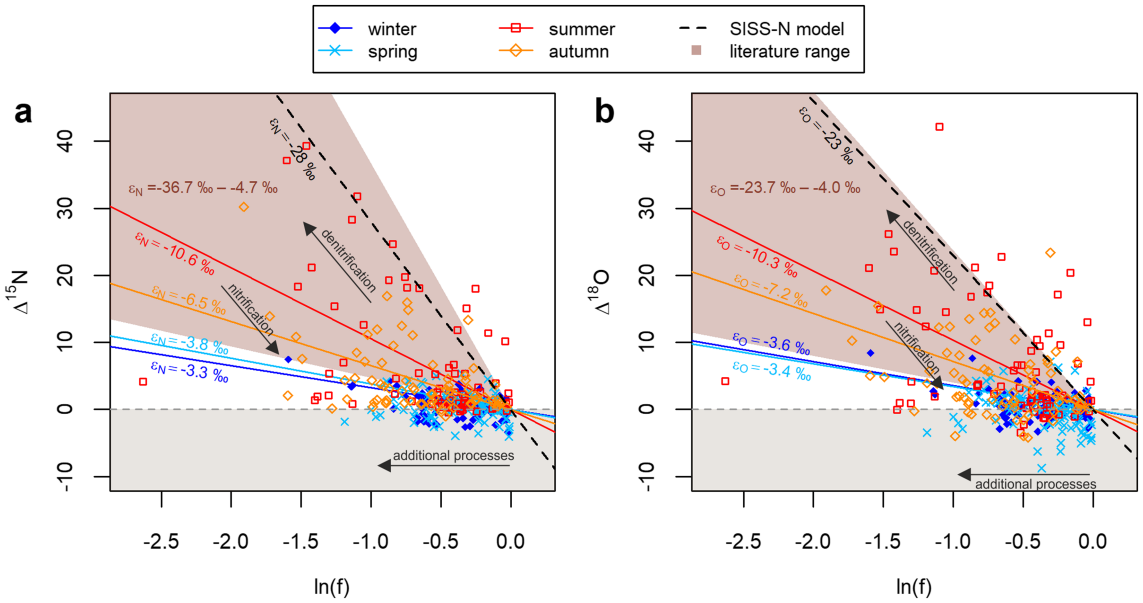

Figure 4. Apparent enrichment factors derived from $\delta^{15}N$ values (a) and $\delta^{18}O$ values (b) for all riparian groundwater samples and different seasons using equation (11) with an intercept of zero and accounting for analytical uncertainties in concentrations and NO_3^- isotope data. $\Delta^{15}N$ and $\Delta^{18}O$ denote the isotopic shifts defined by the left-hand side of equation (11) and *ln*(*f*) is the fraction remaining relative to the theoretical NO_3^- concentration that would result from hydrological mixing only. Samples with negative isotopic shifts were not included in the linear regression. Literature ranges refer to experiments with pure cultures (Barford et al., 1999, Mariotti et al., 1981, Sutka et al., 2006, and Wellman et al., 1968 for ε_N and Granger et al., 2008, Hosono et al., 2015, Knöller et al., 2011, Torrentó et al., 2010, and Wunderlich et al., 2012 for ε_N and ε_O) and are shown as shaded areas between the slopes of minimum and maximum values of ε_N and ε_O, respectively. The directions of changes in *ln*(*f*) and isotopic shifts associated with denitrification, nitrification, and additional processes are indicated by black arrows.

identifying riparian groundwater samples that show evaporation effects in their δ^2H-H_2O and $\delta^{18}O$-H_2O values. To this end, we determined the line-conditioned excess using the stable water isotope data of precipitation and riparian groundwater samples (lc-excess, equation (S2); Landwehr & Coplen, 2006), which is negative for samples affected by evaporation-induced isotope fractionation effects (see Text S3). Using lc-excess < 0 as indicator of evapoconcentration following mixing between river water and groundwater, we reran the model for the subset of riparian groundwater samples with nonnegative lc-excess values (n = 271) and compared the model results to the base scenario.

Table 1
Apparent Isotopic Enrichment Factors From Linear Regression Using Equation (11) and N ($\varepsilon_{N,app}$) and O Isotope Data ($\varepsilon_{O,app}$), Respectively, and Literature Values of Laboratory-Derived Enrichment Factors

Source	ε_N (‰) (R^2)	ε_O (‰) (R^2)
This Study		
Winter	−3.3 (0.8)	−3.6 (0.6)
Spring	−3.8 (0.6)	−3.4 (0.5)
Summer	−10.6 (0.5)	−10.3 (0.5)
Autumn	−6.5 (0.6)	−7.2 (0.6)
Literature		
Barford et al. (1999)	−28.6 ± 1.9	–
Mariotti et al. (1981)	−29.4 ± 2.4	–
Torrentó et al. (2011)	−26.3 ± 1.8	−20.4 ± 1.3
Granger et al. (2008)[a]	−26.6 ± 0.5	−22.6 ± 0.4
Wunderlich et al. (2012)[b]	−23.5 ± 1.9	−23.7 ± 1.8

Note. For the $\varepsilon_{N,app}$ and $\varepsilon_{O,app}$ derived in this study, the coefficients of determination (R^2) are provided in parentheses.
[a]Maximum values among freshwater bacterial strains. [b]Maximum values with acetate as carbon source.

4. Results

4.1. Isotopic Enrichment Factors

The NO_3^- isotope data indicate that apparent isotopic enrichment was generally smaller during winter and spring than during summer and autumn (Figure 4). The isotopic shifts (i.e., $\Delta^{15}N$ and $\Delta^{18}O$) were in the range of a few per mille or even negative (mainly during winter and spring). Linear regression through the origin (i.e., assuming that $\Delta = 0$ if $\ln(f) = 0$) using equation (11) and all riparian samples with positive isotopic shifts yielded the largest isotopic enrichment factors (in terms of absolute values) in summer ($\varepsilon_{N,app} = -10.6‰$ and $\varepsilon_{O,app} = -10.3‰$) and the smallest enrichment factors in winter and spring (i.e., $\varepsilon_{N,app} = -3.3‰$ and $\varepsilon_{O,app} = -3.6‰$ in winter and $\varepsilon_{N,app} = -3.8‰$ and $\varepsilon_{O,app} = -3.4‰$ in spring; Table 1). The $\varepsilon_{N,app}$ and $\varepsilon_{O,app}$ values for winter and spring, in particular, are smaller than ε_N and ε_O values determined from denitrification experiments with pure bacterial cultures (see shaded areas in Figure 4).

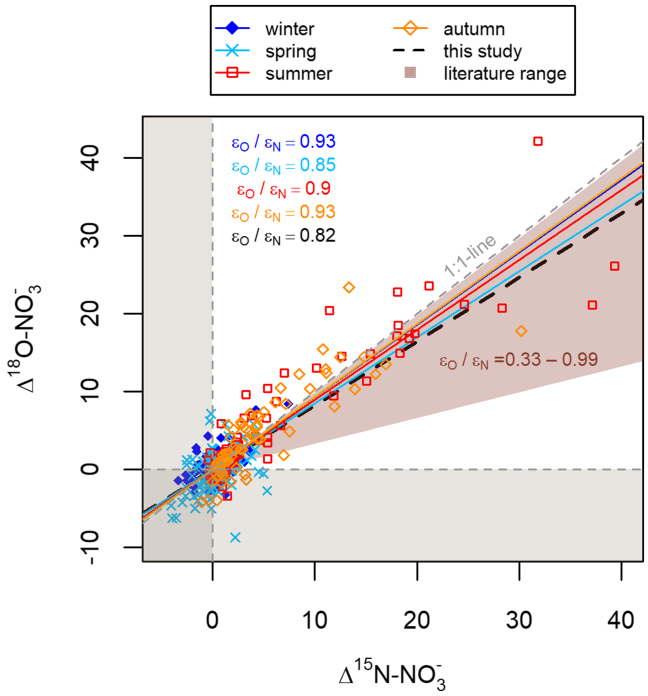

Figure 5. Dual-isotope plot showing isotopic shifts ($\Delta^{18}O\text{-}NO_3^-$ vs. $\Delta^{15}N\text{-}NO_3^-$) for all riparian groundwater samples in different seasons and accounting for analytical uncertainties in concentrations and isotope data. Slopes of $\varepsilon_O/\varepsilon_N$ were determined by linear regression including all points with positive isotopic shifts (i.e., white background). Literature ranges refer to experiments with pure cultures (Granger et al., 2008; Hosono et al., 2015; Knöller et al., 2011; Torrentó et al., 2010; Wunderlich et al., 2012) and are shown as shaded areas between minimum and maximum literature values of $\varepsilon_O/\varepsilon_N$.

We suggest that the samples in Figure 4 indicating significant isotopic enrichment comparable to that found in laboratory studies represent denitrification-induced isotope fractionation with minor impact of additional processes and nitrification. In contrast, samples with $ln(f) < 0$ plotting close to the horizontal lines of $\Delta^{15}N = 0$ or $\Delta^{18}O = 0$ suggest NO_3^- removal without isotope fractionation effects in the remaining NO_3^- pool. This applies, in particular, to the samples taken during winter or spring. Hence, for the following calculations, we adopted ε values at the more negative end of the ranges of laboratory-derived values (Table 1) to describe "pure" denitrification-induced isotope fractionation, that is, $\varepsilon_N = -28.0‰$ and $\varepsilon_O = -23.0‰$. These choices of ε_N and ε_O yield an $\varepsilon_O/\varepsilon_N$ ratio of about 0.82, which is in agreement with Torrentó et al. (2010) and Wunderlich et al. (2012) and aligns well with the seasonal dual-isotope slopes of the riparian groundwater samples (Figure 5).

4.2. Temporal Dynamics of Nitrate Removal

In the following, we refer to the SISS-N model using $\varepsilon_N = -28.0‰$ and $\delta^{15}N\text{-}NO_3^-$ data as the $\delta^{15}N$ model and to the SISS-N model using $\varepsilon_O = -23.0‰$ and $\delta^{18}O\text{-}NO_3$ data as the $\delta^{18}O$ model. Based on the $\delta^{15}N$ model and applying a threshold of 100 simulations with $0 \leq R_{den} \leq 100$, the model calculated R_{den} and R_{add} for 77% of the riparian well samples for which F_{river} was successfully determined ($n = 364$; i.e., 77% of the entire data set). For the remaining samples, the model gave more than 100 simulations with $R_{den} < 0$ because of the theoretical mixture being more enriched in ^{15}N than the riparian groundwater sample (see equation (8)). Using the $\delta^{18}O$ model, R_{den} and R_{add} could be determined for 86% of the samples with valid F_{river}. Despite the larger success rate of the $\delta^{18}O$ model, we present and discuss both model versions for the purpose of comparison and because of the larger analytical uncertainty in $\delta^{18}O$ values relative to their isotopic enrichment compared to $\delta^{15}N$ values.

We present the temporal dynamics of NO_3^- removal separately for the near and the intermediate groundwater zones (wells with a distance of <25 and 25–55 m, respectively, from the river; see Figure 1). In the near groundwater, mean NO_3^- removal via denitrification (R_{den}) was 11.5% ± 14.9% and mean NO_3^- removal by

Table 2
Overall NO_3^- Removal (R_{tot}), Denitrification (R_{den}), and Removal by Additional Processes (R_{add}) in the Base Scenario, the Extreme Scenario With Maximum Denitrification in Groundwater ($R_{tot,ext}$, $R_{den,ext}$, and $R_{add,ext}$) and for the Sample Subset With Nonnegative lc-Excess ($R_{tot,lc}$, $R_{den,lc}$, and $R_{add,lc}$).

	Near groundwater		Intermediate groundwater	
	$\delta^{15}N$	$\delta^{18}O$	$\delta^{15}N$	$\delta^{18}O$
Base Scenario				
R_{den} (%)	11.5 ± 14.9	15.6 ± 15.0	6.1 ± 9.7	9.8 ± 9.6
R_{add} (%)	26.7 ± 19.0	22.2 ± 18.8	26.7 ± 13.9	24.1 ± 13.7
R_{tot} (%)	37.7 ± 21.8	36.3 ± 22.2	32.7 ± 15.1	33.4 ± 15.1
Max. Denitrification in Groundwater				
$R_{den,ext}$ (%)	27.0 ± 36.3	36.6 ± 33.4	6.6 ± 11.2	11.5 ± 13.3
$R_{add,ext}$ (%)	21.7 ± 20.8	16.4 ± 19.2	26.5 ± 14.1	22.2 ± 13.3
$R_{tot,ext}$ (%)	37.7 ± 21.9	37.7 ± 21.9	32.7 ± 15.1	32.4 ± 15.1
Samples With lc-Excess ≥ 0				
$R_{den,lc}$ (%)	12.0 ± 15.6	15.9 ± 15.4	6.2 ± 10.1	10.3 ± 10.2
$R_{add,lc}$ (%)	26.0 ± 18.8	21.3 ± 18.5	26.9 ± 14.2	23.8 ± 14.3
$R_{tot,lc}$ (%)	37.4 ± 21.8	35.7 ± 22.2	32.9 ± 15.7	33.5 ± 15.9

Note. Values are given as mean ± standard deviation of the sample subset with $R_{den} \geq 0$, $R_{den,ext} \geq 0$, or $R_{den,lc} \geq 0$, respectively, after setting negative R_{add} values to zero. Samples with less than 100 successful Monte Carlo simulations were discarded. R_{tot} differs between the $\delta^{15}N$ and $\delta^{18}O$ models and between the model scenarios as the statistics refer to different sample subsets. being set to zero for further calculations, R_{add} values < 0 are explicitly shown in this figure.

additional processes (R_{add}) was 26.7% ± 19.0%, resulting in a mean total removal (R_{tot}) of 37.7% ± 21.8% using the $\delta^{15}N$ model (Table 2). In the near groundwater, the mean R_{add} was thus more than twice as large as the mean R_{den} during the study period. In terms of temporal variations, denitrification showed a clear relationship with groundwater temperature, with larger values during summer and autumn than during winter and spring (Figure 6a). Considering the median value of all wells per sampling date using

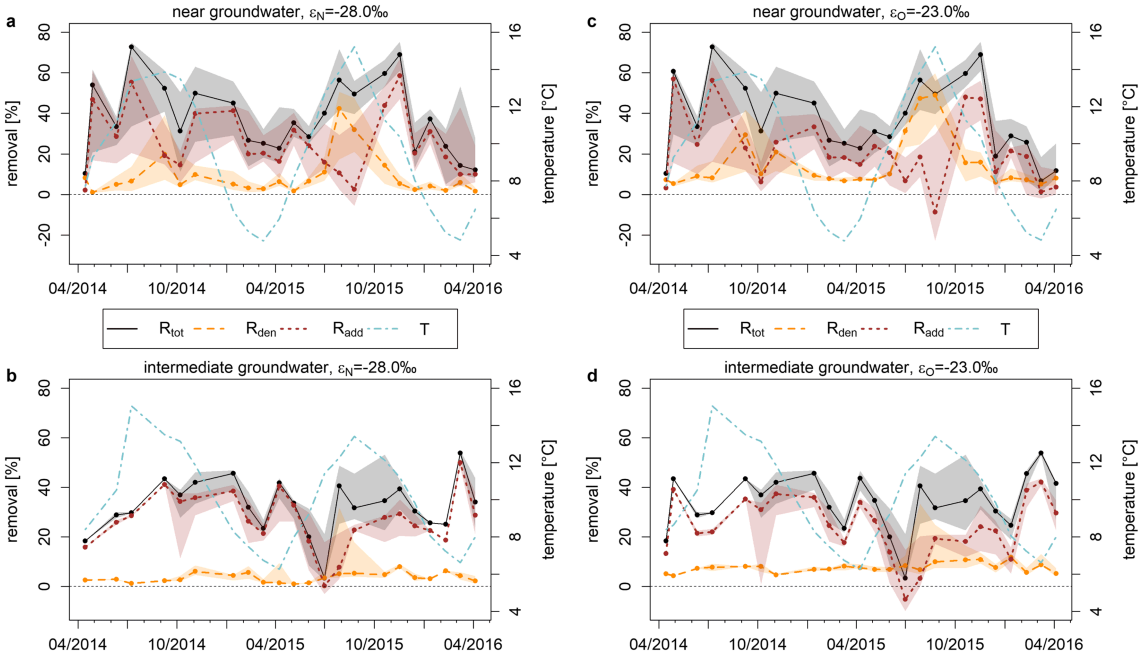

Figure 6. Nitrate removal (%; median of all wells) in the riparian wells in the near (upper panels) and intermediate groundwater (lower panels) using N isotope data with $\varepsilon_N = -28.0‰$ (left panels) and O isotope data with $\varepsilon_O = -23.0‰$ (right panels). Total NO_3^- removal (R_{tot}) is shown as solid black line, the extent of denitrification (R_{den}) as dashed orange line, and removal by additional processes (R_{add}) as dotted brown line. Shaded areas indicate the 25% to 75% quantile ranges of R_{tot} (grey), R_{den} (orange), and R_{add} (brown). The dash-dotted blue line indicates the mean temperature at the wells in the respective groundwater zone. While being set to zero for further calculations, R_{add} values < 0 are explicitly shown in this figure.

the $\delta^{15}N$ model, R_{den} ranged between 1.1% in April 2014 and 42.3% in July 2015, while the median R_{add} ranged between 2.2% in April 2014 and 58.6% in November 2015.

With a mean value of $R_{tot} = 32.7\% \pm 15.1\%$ using the $\delta^{15}N$ model, total NO_3^- removal was smaller in the intermediate than in the near groundwater (Table 2). The model attributed most of NO_3^- removal in the intermediate groundwater to R_{add} (mean of $26.7\% \pm 13.9\%$), while R_{den} was, on average, by a factor of 4 smaller than R_{add} (mean of $6.1\% \pm 9.7\%$) and less pronounced than in the near groundwater. In terms of temporal variations, there was no pronounced increase in denitrification during summer and autumn, as opposed to the dynamics in the near groundwater. The median R_{den} of all wells per sampling date ranged between 1.0% in May 2015 and 8.0% in November 2015 using the $\delta^{15}N$ model (Figure 6b). In contrast, the median R_{add} of all wells ranged between 0.3% in July 2015 and 50.0% in March 2016 and was mostly above 15%.

Using the $\delta^{18}O$ model, the extent of denitrification increased compared to the results of the $\delta^{15}N$ model (Table 2), yielding a range from 5.1% in March 2016 to 49.0% in August 2015 for the median R_{den} in the near groundwater (Figure 6c) and a range from 4.4% in April 2014 to 11.8% in January 2016 for the median R_{den} in the intermediate groundwater (Figure 6d). Denitrification in the near groundwater was most pronounced during summer and autumn, whereas there was no clear seasonal pattern for R_{den} in the intermediate groundwater (albeit its range increased during summer 2015; Figure 6d). This is in line with the seasonal R_{den} patterns calculated with the $\delta^{15}N$ model. While R_{den} increased using the $\delta^{18}O$ model, the removal by additional processes decreased compared to the $\delta^{15}N$ model results (Table 2). In terms of temporal dynamics, the median R_{add} of all wells ranged between 0% and 56.9% in the near groundwater (Figure 6c) and between 0% and 42.1% in the intermediate groundwater (Figure 6d).

In summary, using the median values per sampling date from the $\delta^{15}N$ model, the relative contribution by R_{den} to overall NO_3^- removal (i.e., sum of R_{den} and R_{add}) ranged over time from 4.7% to 95.1% (mean of $29.0\% \pm 24.4\%$) in the near groundwater and from 2.8% to 91.2% (mean of $16.7\% \pm 18.2\%$) in the intermediate groundwater. Moreover, the base scenario suggests that average NO_3^- removal by additional processes exceeded denitrification, at least, by a factor of 1.4 in the near groundwater and by a factor of 2.5 in the intermediate groundwater (Table 2). Third, the $\delta^{15}N$ model generally yielded smaller R_{den} and, therefore, larger R_{add}-values than the $\delta^{18}O$ model. Nonetheless, the mean R_{add} using the $\delta^{18}O$ model differed from the mean R_{add} using the $\delta^{15}N$ model by less than 5% (in absolute terms) for both the near and intermediate groundwater (Table 2). Similarly, the absolute difference between the mean R_{den} values from the two models was around 4% in both groundwater zones. Notwithstanding the differences in the mean, the temporal dynamics in both groundwater zones are generally consistent between the $\delta^{15}N$ and the $\delta^{18}O$ models (Figure 6).

4.3. Spatial Patterns of Nitrate Removal

Given the consistency in temporal patterns of the two models, we present the results of the $\delta^{15}N$ model in the following and provide the results of the $\delta^{18}O$ model in the supporting information (Text S4 and Figure S4). To analyze spatial patterns of seasonal dynamics in NO_3^- removal, we calculated R_{den} and R_{add} of each well separately for the summer and winter months. Averaged over the summer months in 2014 and 2015, R_{den} at individual wells ranged between 1.1% and 55.8% (mean of $21.8\% \pm 17.5\%$; Figure 7a). Denitrification was most pronounced at C-N and C-S and smallest at A and B-N. In contrast, NO_3^- removal by additional processes during summer was largest at B-N and smallest at C-S (Figure 7b). The model yielded a mean (maximum) R_{add} of $22.0\% \pm 15.6\%$ (50.4%) and $R_{add} = 0$ for one C-S well during summer.

The extent of denitrification during winter months (Figure 7c) was substantially smaller than during summer months and never exceeded R_{tot}, as opposed to one C-S well in summer. The mean R_{den} at all wells was $4.5\% \pm 3.2\%$ (range from 1.3% to 14.9%; Figure 7c) and, in contrast to the summer months, R_{den} was below 9% in all transects apart from one well at C-N with $R_{den} = 14.9\%$. Mean removal by additional processes during winter was $R_{add} = 27.3\% \pm 12.2\%$ (range from 7.8% to 51.3%; Figure 7d). In contrast to denitrification, additional processes accounted for pronounced removal in the A and B transects and some of the C transect wells. In summary, R_{add} during winter was high at most B transect wells, while the smallest R_{add} values occurred in the C transect.

Overall, R_{den} was substantially larger during summer than winter, whereas R_{add} values were comparable during both seasons (Figure 7). During summer, R_{den} was at a similar level as R_{add}, whereas it was largely

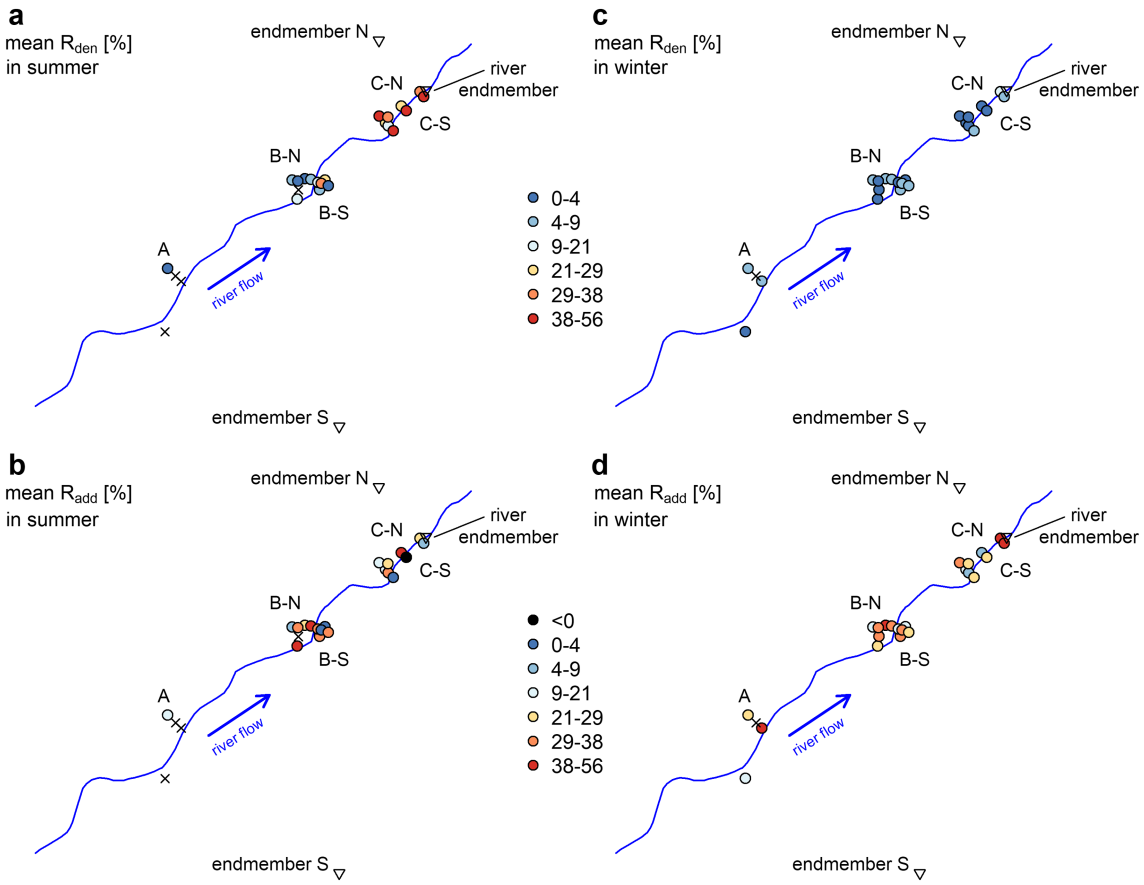

Figure 7. Mean NO_3^- removal (%) in summer (left panels) and winter (right panels) by denitrification (R_{den}, upper panels) and additional processes (R_{add}, lower panels) at the riparian wells using nitrogen isotope data with $\varepsilon_N = -28.0‰$. Dot colors range from blue to red (small to large values) for R_{den} and R_{add}, with black dots indicating negative R_{add} values. The marker "x" represents wells for which NO_3^- removal could not be calculated due to missing NO_3^- isotope values or an insufficient number of valid SISS-N model results. Letters A, B-N, B-S, C-N, and C-S indicate the different well clusters shown in Figure 1b. While being set to zero for further calculations, R_{add} values < 0 are explicitly shown in this figure.

exceeded by R_{add} during winter. Considering the mean values with the $\delta^{15}N$ model over the entire study period (not shown), R_{den} was largest mainly in the C transect (above 75th percentile of 15.9%) and smallest in the A and B-N transects (below 25th percentile of 4.8%). In contrast, R_{add} was largest at B-N (above 75th percentile of 31.5%) and smallest at B-S and C (below 25th percentile of 23.6%). These spatial patterns of R_{den} and R_{add} were similar using the $\delta^{18}O$ model (Text S4 and Figure S4), thereby highlighting some wells of clusters C and B as hotspots of denitrification and additional NO_3^- sinks, respectively.

4.4. Additional Model Scenarios

The occurrence of denitrification for the groundwater end-member prior to mixing was assessed by the scenario assuming maximum R_{den} for the groundwater end-member (Figure S2). The percentage of samples for which $R_{den,ext}$ exceeded R_{tot} increased from 4.6% in the base scenario to 21.7% in the extreme scenario using the $\delta^{15}N$ model. Correspondingly, the extreme scenario yielded substantially larger denitrification estimates (especially in the near groundwater) and somewhat smaller estimates of NO_3^- removal by additional processes compared to the base scenario (i.e., $R_{den,ext} > R_{den}$ and $R_{add} > R_{add,ext}$; Table 2). In the near groundwater, mean denitrification increased from R_{den} = 11.5% ± 14.9% in the base scenario to $R_{den,ext}$ = 27.0% ± 36.3%, whereas removal by additional processes decreased from R_{add} = 26.7% ± 19.0% in the base scenario to $R_{add,ext}$ = 21.7% ± 20.8% (Table 2). In the intermediate groundwater, the extent of denitrification slightly increased from R_{den} = 6.1% ± 9.7% to $R_{den,ext}$ = 6.6% ± 11.2%, while NO_3^- removal by additional processes marginally decreased from R_{add} = 26.7% ± 13.9% to $R_{add,ext}$ = 26.5% ± 14.1%.The same

tendency of increasing $R_{den,ext}$ and decreasing $R_{add,ext}$ compared to the base scenario became also apparent using the $\delta^{18}O$ model (especially in the near groundwater).

In the second additional scenario, we applied the SISS-N model to those riparian groundwater samples with lc-excess ≥ 0 in order to exclude samples that might have been significantly affected by evaporation (Text S3 and Figure S3). Using negative lc-excess values as indicator of enhanced evaporation, potential evapoconcentration effects in riparian groundwater might have particularly occurred during April and June 2014 and April 2015 (not shown). Nonnegative lc-excess values for riparian groundwater samples occurred for 85.7% of all valid SISS-N model runs. For this subset, F_{river} was similar to that in the base scenario (i.e., mean of 0.64 ± 0.33 vs. 0.65 ± 0.33) and overall NO_3^- removal was nearly identical to that in the base scenario (i.e., using the $\delta^{15}N$ model, $R_{tot,lc}$ = 37.4% ± 21.8% vs. R_{tot} = 37.7% ± 21.8% in the near groundwater, and $R_{tot,lc}$ = 32.9% ± 15.7% vs. R_{tot} = 32.7% ± 15.1% in the intermediate groundwater; Table 2). Moreover, the scenario yielded overall slightly larger denitrification estimates and slightly smaller estimates of removal by additional processes in both groundwater zones (Table 2), with maximum deviations of around 1% (in absolute values) between mean $R_{den,lc}$ and mean R_{den} and between mean $R_{add,lc}$ and mean R_{add}, respectively.

5. Discussion

5.1. Isotope Fractionation and Enrichment Factors

The isotopic enrichment factors of $\varepsilon_N = -28.0‰$ and $\varepsilon_O = -23.0‰$ chosen in this study lie at the more negative end of the range reported previously (i.e., indicating larger isotope effects; Table 1). This implies that the model results represent conservative estimates of denitrification at the field site. In other words, assuming less pronounced isotope fractionation (i.e., less negative values of ε_N and ε_O) would result in larger R_{den} values and thus smaller R_{add} values. As this would have given more instances of $R_{add} < 0$ even in the conservative base scenario (assuming accurate R_{tot} estimates), we suggest that $\varepsilon_N = -28.0‰$ and $\varepsilon_O = -23.0‰$ accurately describe denitrification-induced isotopic fractionation that is not diluted by the occurrence of nonfractionating processes, in contrast to apparent isotopic enrichment factors derived from field isotope data. Hence, in addition to quantifying the contribution of denitrification to overall NO_3^- removal, combining concentration and isotope data such as in the SISS-N model can help delimit a plausible range for isotopic enrichment factors under field conditions.

In addition to the Rayleigh plot (Figure 4), the $\varepsilon_O/\varepsilon_N$ slope in the dual-isotope plot (Figure 5) can provide more insights into the magnitude of ε_N and ε_O at our field site. In contrast to Rayleigh plots, dual-isotope plots have the advantage of being unaffected by concentration decreases due to nonfractionating processes. While matching the upper quartile of the literature range (i.e., 0.33 to 0.99; Granger et al., 2008; Hosono et al., 2015; Knöller et al., 2011; Torrentó et al., 2010; Wunderlich et al., 2012), the $\varepsilon_O/\varepsilon_N$ slope of 0.82 as assumed here is less steep than the seasonal $\varepsilon_O/\varepsilon_N$ slopes derived from the riparian groundwater samples (e.g., maximum $\varepsilon_O/\varepsilon_N$ of 0.93 during winter and autumn; Figure 5). This might result from underestimation of the actual ε_O or overestimation of the actual ε_N (in terms of absolute values). A larger ε_O would result in smaller R_{den} values with the $\delta^{18}O$ model and could thus reduce instances of $R_{add} < 0$ (Figures 6c, 6d, and S4b). Moreover, deviations from the 1:1 slope in the dual-isotope plot might also indicate addition of newly nitrified NO_3^- or NO_3^- produced by anammox (Granger & Wankel, 2016). The fact that we cannot conclusively determine what processes in addition to denitrification might affect the field isotope data is another reason why we employed ε values in agreement with studies using isolated bacterial cultures instead of apparent ε values derived from our field data.

The concurrent isotopic enrichment in $\delta^{15}N$ and $\delta^{18}O$, associated with decreasing NO_3^-concentrations between spring and summer (Figures 2c–2e), suggests the occurrence of denitrification in the riparian zone, as opposed to changes in source isotope values, which are not likely to entail concurrent enrichment in $\delta^{15}N$ and $\delta^{18}O$. In contrast, the lack of isotope fractionation in the river (based on differences in the isotopic composition between upstream and downstream sampling points; Table S1) suggests that in-stream denitrification along the 2 km reach at our field site was negligible. Hence, while in-stream denitrification can be significant at the river-network scale (Seitzinger et al., 2002), we focused here on the analysis of NO_3^- removal from riparian groundwater and neglected potential in-stream removal processes.

5.2. Quantification of Denitrification

The SISS-N model results highlight pronounced temporal changes in the importance of different NO_3^- removal processes, which complicates a comparison of our estimates to those from previous studies that have assessed denitrification over the course of a few months only (Dhondt et al., 2003;Jahangir et al., 2017 ; McPhillips et al., 2015). Nonetheless, our results underline substantial differences in the extent of denitrification between near and intermediate groundwater, and suggest that additional processes other than denitrification govern NO_3^- removal at our field site. This is in line with previous studies such as McPhillips et al. (2015), who calculated a contribution of 29%–69% to overall NO_3^- removal by plant uptake, abiotic immobilization, and microbial assimilation, and Jahangir et al. (2017), who assessed a relative contribution of 40%–63% by DNRA. Note that while R_{den} in the near groundwater is generally larger than R_{den} in the intermediate groundwater, this does not necessarily apply to absolute values of NO_3^- removal via denitrification, as these depend on the NO_3^- fluxes through the respective groundwater zones.

Denitrification in the near groundwater increased with rising groundwater temperatures in summer (Figures 6a and 6c), which agrees with the strong temperature dependency of denitrification reported previously (Pfenning & McMahon, 1997; Saunders & Kalff, 2001; Stanford et al., 1975). However, denitrification in the intermediate groundwater was limited despite similar temperatures as in the near groundwater, which corroborates the relevance of additional factors for denitrification such as the presence of organic carbon provided by infiltrating river water (Trauth et al., 2018). Dissolved organic carbon concentrations in the river were indeed more than twice as high as in distant groundwater (Table S1). Provided that mixing between distant groundwater and river water governs the hydrochemistry in riparian groundwater, this indicates the importance of the river as organic carbon source, either directly via in-stream primary production (Dupas et al., 2017) or indirectly via hydrological connectivity between rivers and wetland soils rich in organic carbon (Lambert et al., 2011; Shang et al., 2018). The importance of DOC provided by the river becomes apparent in the spatial analysis, which yielded the largest summer R_{den} at the B-S and C transects (Figure 7a). Those are the well clusters for which F_{river} indicates significant inflow of river water (Figure 1b), as opposed to the A and B-N transects, for which our model calculated smaller R_{den} values. This suggests that denitrification depends to a greater extent on the exchange with surface water than on subsurface properties such as the varying thickness of the alluvial aquifers (see Vidon & Hill, 2004) north and south of the river (Figure 1c). In addition to hydraulic conditions, northern and southern wells differed in their NO_3^- concentration levels, with concentrations of the southern groundwater end-member being, on average, 4.5 times as high as those of the northern groundwater end-member (Figure 2c). As denitrification potential is generally positively correlated with NO_3^- concentrations (Ahn & Peralta, 2012; Seitzinger, 1994), this might further explain the larger R_{den} values south of the river (Figures 7a and 7c).

The variability in $\delta^{15}N$ and $\delta^{18}O$ values in the more distant groundwater wells south of the river do not indicate systematic isotopic enrichment associated with denitrification (Text S6 and Figure S7). Nonetheless, using the extreme scenario of maximum denitrification for the groundwater end-member, we were able to assess how denitrification during flow from the groundwater end-member to the riparian zone might affect the estimates of total denitrification. The $R_{den,ext}$ estimates in valid simulations of this scenario were considerably larger than R_{den} (Table 2), which demonstrates that the base scenario gives a conservative estimate of the extent of denitrification and, hence, of permanent NO_3^- removal from riparian groundwater. Nonetheless, before setting them to zero, $R_{add,ext}$ values were frequently in the double-digit negative range, which highlights that this scenario likely heavily overestimates $R_{den,ext}$ especially in the near groundwater where isotope fractionation was more pronounced. In reality, considering the role of organic carbon from river water, the denitrification potential in groundwater flowing from the distant groundwater to the river is likely smaller than that in the riparian zone. Moreover, even in this extreme scenario, $R_{add,ext}$ substantially contributed to overall NO_3^- removal (i.e., amounting to around 55% and 77% of $R_{tot,ext}$ in the near and intermediate groundwater, respectively, using the $\delta^{15}N$ model).

5.3. Nitrate Removal by Additional Processes

Among the biotic NO_3^- consumption processes, DNRA is a process that might lead to a similar extent of NO_3^- removal as denitrification (Jahangir et al., 2017; McPhillips et al., 2015). Microbial transformation via DNRA occurs (such as denitrification) under anaerobic and reduced conditions and is favored over

denitrification when C:N ratios are large (Dhondt et al., 2003; Jahangir et al., 2017; Matheson et al., 2002). However, in our study, the mean C:N ratio using the molar concentrations of DOC and N-NO_3^- of the six wells with the largest R_{add} (i.e., above the 75th percentile) was smaller than that of the six wells with the largest R_{den} (i.e., 1.0 vs. 1.5 using the $\delta^{15}N$ model). Moreover, wells with large R_{add} values generally showed elevated E_h values, unlike the wells with large R_{den} values (i.e., means of 58.0 and 175.0 mV for the six wells with the largest R_{den} and largest R_{add}, respectively, and 132.1 mV for all riparian wells). Third, concentrations of NH_4^+ (i.e., the reaction product of DNRA) did not exceed 0.55 mg L^{-1} and were mostly below detection limit (0.02 mg L^{-1}) in riparian groundwater. Overall, a substantial contribution of DNRA to NO_3^- consumption during the study period at our field side is thus unlikely.

In contrast to R_{den}, R_{add} is of similar magnitude in the near and intermediate groundwater zones (Figure 6). A potential NO_3^- sink that does not show a significant gradient with distance from the river is riparian vegetation. In general, although Clément et al. (2003) suggested that plants primarily use riparian groundwater during high flow conditions, the common assumption is that NO_3^- uptake by plants mainly occurs from late spring to autumn during the growing season (Li et al., 2016; Muñoz et al., 1993). This is consistent with the positive relationship of R_{add} with temperature in the intermediate groundwater (Figures 6b and 6d) and the slightly larger R_{add} in summer compared to winter (Figures 6 and 7). However, these relationships might as well indicate increased microbial NO_3^- removal under warm conditions. In addition, as the additional processes were also active during the dormant season, plant uptake cannot be the only major NO_3^- sink besides denitrification at our field site.

A mechanism that is potentially active during winter is the abiotic immobilization of NO_3^- into soil organic matter following reaction with Fe^{2+} species (Davidson et al., 2003; McPhillips et al., 2015). Although challenged by Colman et al. (2007), this pathway has been assumed to be a major NO_3^- sink in forest soils (Judd et al., 2007; Providoli et al., 2006). Ferrous iron at our field site was detectable only in a few cases in groundwater, making it impossible to assess whether this process might also play a role in the riparian zone. In addition to abiotic immobilization, microbial assimilation of NO_3^- might be an important additional NO_3^- sink, particularly during winter time (Dhondt et al., 2003). Nitrate uptake has, for example, been reported by cyanobacteria in groundwater (Hu et al., 2000) and benthic algae in a mountainous stream (Baker et al., 2009). A detailed study on microbial NO_3^- uptake would be necessary in order to assess the role of this pathway relative to other NO_3^- sinks. This is not feasible based on our data and goes beyond the scope of this study.

Provided that the overall assessment of R_{add} is adequate, our results indicate that NO_3^- removal by processes other than denitrification might play a significant role in riparian zones (Clément et al., 2003; Davis et al., 2008; Dhondt et al., 2003; McPhillips et al., 2015), particularly if enrichment factors associated with denitrification are comparably large under field as under laboratory conditions. As additional removal processes result in nitrogen retention in riparian zones rather than in permanent nitrogen loss to the atmosphere, attributing NO_3^- consumption to denitrification exclusively might greatly overestimate the capacity of riparian ecosystems for permanent NO_3^- removal in similar systems. Hence, we assume that our results might be, in particular, transferable to river sections where groundwater flow similarly dominates streamflow generation and organic carbon supply to groundwater relies on the interaction between stream water and groundwater. Our data do not allow unequivocally identifying individual NO_3^- consumption processes or inferring their relative contribution to total NO_3^- removal from groundwater. We suggest that microbial and abiotic immobilization and plant uptake are the potential main contributors to NO_3^- removal at our field site, while DNRA presumably plays a minor role. This information is also relevant for future studies as it highlights what processes and parameters have to be investigated in more detail with regard to isotope analyses and riparian NO_3^- consumption (e.g., the measurement of sulfur and dissolved inorganic carbon isotopes; Hosono et al., 2015; Otero et al., 2009).

5.4. Uncertainties and Limitations

During times of hydrological connectivity between soil and riparian groundwater, soil NO_3^- carrying the isotopically depleted imprint of nitrification can leach to shallow riparian groundwater (Clément et al., 2003; Hall et al., 2016). Consequently, as indicated in Figure 4, vertical mixing with freshly nitrified NO_3^- might shift isotopic signatures toward larger ln(f)-values and smaller $\Delta^{15}N$ and $\Delta^{18}O$ than would occur for

denitrification only. The isotopic signature of nitrified NO_3^- depends on the isotopic signatures of NH_4^+ and O from water and atmosphere as well as varying isotope fractionation effects during nitrification (Granger & Wankel, 2016; Kendall et al., 2007). Hence, we cannot readily quantify the isotopic shift associated with nitrification and, accordingly, neither its effect on the assessment of isotopic enrichment factors in this study. However, for our field site, we consider it safe to assume that NO_3^- stems for the most part from surrounding arable land and the contribution of freshly nitrified NO_3^- from riparian soils to groundwater NO_3^- is minor. Provided that nitrification in the riparian zone plays a significant role, the SISS-N model yields conservative estimates of denitrification as nitrification can partially mask denitrification-induced isotope fractionation (Hall et al., 2016; Wexler et al., 2014). Moreover, data points plotting to the right and top of the shaded area in Figures 4a and 4b (i.e., larger ln(f) and Δ values) might be affected by addition of manure or NO_3^- fertilizers, which are generally more enriched in ^{15}N and ^{18}O, respectively, than NO_3^- originating from NH_4^+ fertilizers. Similar to nitrification, the effect of additional sources cannot readily be assessed without detailed information on source signatures and associated NO_3^- loads.

A crucial model assumption is that denitrification is the only NO_3^- sink entailing significant isotope fractionation at the field site. Data on potential isotope fractionation effects associated with additional processes are scarce or not available, in contrast to the extensively studied fractionation effects accompanying denitrification. In the case of DNRA, for example, the occurrence or extent of isotope fractionation is unknown to date (Nikolenko et al., 2018). However, given it is a microbially mediated NO_3^- reduction process such as denitrification, DNRA might also cause significant isotopic enrichment in the remaining NO_3^-. Similarly, in agreement with Dhondt et al. (2003) who measured enrichment factors of $\varepsilon_N = -4.4‰ \pm 0.3‰$ in hydroponics, plant uptake has been generally associated with minor isotope fractionation compared to denitrification (Denk et al., 2017; Högberg et al., 1999; Lund et al., 1999). In contrast, recent enzymatic assays using eukaryotic NO_3^- assimilatory reductases (Karsh et al., 2012; Treibergs & Granger, 2017) have reported ε_N and ε_O values as large as ≈30‰. Nonetheless, we are not able to assess either the transferability of such enzyme-level isotope effects to field conditions or the role of the associated eukaryotes for NO_3^- removal at the field site.

The accuracy of R_{tot} is, in part, affected by the temporal resolution of our data, considering that monthly data do not allow capturing short-term variations in NO_3^- production and transformation (and potential associated fractionation processes) in the riparian zone. Second, uncertainties in R_{tot} result from the assumption of instantaneous end-member mixing and are thus inherited from the concentration-based mixing model via the calculation of F_{river} (equation (2)) and [$NO_3^-{}_{mix}$] (equation (3)). The assumption of instantaneous mixing is valid as long as travel times from the end-members to the riparian zone are short or end-member concentrations and isotope values remain stable over time. Considering that the distant groundwater has to travel a longer distance to the riparian zone than river water, these restrictions might be more problematic for the groundwater end-member than for the river end-member. The uncertainties related to the assumption of instantaneous mixing are particularly critical for the southern groundwater end-member, which shows a downward NO_3^- concentration trend (but no distinct trend in isotope values) over the study period (Figure 2c). If we were to account for a certain travel time from the distant groundwater to the riparian zone, we would have to increase the concentration of the southern groundwater end-member in the SISS-N model according to the decreasing concentration trend. This would lead to larger $NO_3^-{}_{mix}$ values in equation (4) and thus to larger R_{tot} and R_{add} values. However, estimates of flow velocities in the southern groundwater using the Darcy equation (assuming similar hydraulic properties as reported in Gassen et al., 2017 for the riparian zone) suggest flow velocities of around 5 m day^{-1} and thus comparably short travel times to the riparian zone. We, therefore, consider the uncertainties associated with the assumption of instantaneous mixing to be small compared to model applications for systems with less permeable aquifers.

Evapoconcentration of Cl^- in riparian groundwater samples might lead to a bias in F_{river} toward the groundwater end-members, as the Cl^- concentrations of the groundwater end-members (especially south of the river) were higher than those of the river end-member (Figure 2b). Similarly, evapoconcentration might result in larger NO_3^- concentrations measured in riparian groundwater and thus smaller R_{tot} and R_{add} estimates. Using lc-excess < 0 as indicator of increased evaporation, the fraction of riparian groundwater samples for which the SISS-N model might be affected by evaporation-induced isotope fractionation was around 14%. However, F_{river} for the subset of samples with lc-excess ≥ 0 was nearly identical to F_{river} in the base

scenario, indicating a minor impact of potential evapoconcentration effects on the results of the Cl^- mixing model. Correspondingly, application of the SISS-N model to this subset yielded deviations of below 1% between mean $R_{tot,lc}$ and mean R_{tot} and minor differences in mean $R_{den,lc}$ and mean $R_{add,lc}$ from the base scenario results (Table 2). Hence, although evapoconcentration effects might have played a role for some samples, we can assume that the SISS-N model results remained largely unaffected by these.

While evapoconcentration appears to play a minor role, there might be other factors leading to the considerable amount of invalid F_{river} values (i.e., 23% of all samples) and thus to failure of the chloride mixing model. For example, addition of Cl^- from potassium chloride fertilizers during flow from the distant groundwater to the riparian zone might increase Cl^- concentrations above the end-member concentrations and thus lead to negative F_{river} values (see equation (2)). Moreover, $F_{river} < 0$ mostly occurs in the northern groundwater zone, for which we chose a groundwater well on the western fringe of the field site as distant groundwater end-member, which might not fully represent all wells north of the river. The opposite effect of $F_{river} > 1$ is mainly associated with sample concentrations below the end-member concentrations and might result from dilution in the riparian zone via an additional source with low Cl^- concentrations such as rapid infiltration of rainwater in the riparian zone. The latter scenario would also imply dilution of NO_3^- concentrations in the riparian zone. While we cannot exclude the presence of an unknown third end-member, the requirement of $0 \leq F_{river} \leq 1$ enables us to restrict the analysis to samples for which such uncertainties do not majorly affect the model results.

5.5. Recommendations for Future Model Applications

We restricted our model to two mixing end-members as the study site is dominated by groundwater flow, and runoff generation via shallow soil flow paths is not significant. In more "flashy" systems where shallow flow paths become active during rainfall events, it might be required to add a third end-member to represent a hydrochemically disparate soil layer that temporally plays a substantial role for stream water chemistry (e.g., in steep headwater catchments; Seibert et al., 2009; Zhi et al., 2019), provided that this soil end-member significantly differs from the other two in its Cl^- or NO_3^- concentrations or NO_3^- isotope values. In such cases, river water during high-flow conditions represents a mixture of deeper groundwater and more shallow soil flow paths. Hence, unlike in our model application, it might be necessary to characterize the hydrochemistry of shallow riparian soil and amend the mixing equations such that river water results from mixing between the soil and groundwater signatures for ion concentrations and isotope values.

The minimum data requirements for application of the SISS-N model to assess NO_3^- removal from riparian groundwater are concentration data of chloride (or another conservative tracer), and concentration and N (or O) isotope data of NO_3^-. These data should be measured in the stream, distant groundwater, and one or several riparian groundwater wells, ideally at least at monthly resolution during one year to assess seasonal dynamics. If the dual-element isotope values of the end-members are associated with small analytical uncertainties and sufficiently differ from each other, it is also possible to apply the original SISS model and calculate R_{den} solely from the $\delta^{15}N\text{-}NO_3^-$ and $\delta^{18}O\text{-}NO_3^-$ data. This might, in fact, be advisable if the end-member concentrations of the conservative tracer are similar and thus introduce high uncertainties in the calculation of end-member contributions via the linear mixing model. However, the original SISS model does not provide R_{tot} estimates and, therefore, does not obviate the use of a mixing model using tracer and NO_3^- concentrations to quantify overall NO_3^- removal from riparian groundwater.

The SISS-N model cannot provide any information additional to conventional end-member mixing models in the absence of significant isotope fractionation at the field site. However, it is not straightforward to specify a threshold above which apparent isotope fractionation can actually be considered significant, as the extent of denitrification associated with a certain isotopic shift depends on the underlying isotopic enrichment factor. Fortunately, the SISS-N model allows testing the plausibility of different enrichment factors with little computational effort. Hence, it is not necessary to decide a priori whether isotope fractionation at a field site should be considered as significant, as long as there is some reasonable estimate of the "true" enrichment factor associated with pure denitrification at the field site.

The choice of ε values has significant impact on the SISS-N model results, as well as on any other model using field isotope data to assess denitrification. Hence, based on this study, we suggest (i) a thorough comparison of field-derived maximum ε values and literature values and (ii) testing of ε values against the

prerequisite $R_{add} \geq 0$ in order to reduce the uncertainties associated with the choice of isotopic enrichment factors. If a field site shows evidence of fractionating NO_3^- removal processes besides denitrification, the SISS-N model can be driven with a bulk enrichment factor combining estimates of the isotope fractionation effects via denitrification and additional processes. Such a model would be comparable to the approach in Dhondt et al. (2003) for denitrification and plant uptake and additionally account for mixing processes in the riparian zone. Including additional fractionating processes while assuming the same ε-values for denitrification as before would result in a smaller contribution of denitrification to overall NO_3^- removal, as the same isotopic enrichment would be attributed to fractionation effects by denitrification and other processes. In contrast, the model estimate of NO_3^- removal by nonfractionating processes (R_{add}) would remain unaffected by additional fractionating processes.

The uncertainty analysis indicated a minor role of evapoconcentration effects at our field site. However, under conditions of significant evapoconcentration, one would first have to correct the Cl^- and NO_3^- concentrations of the mixture in the riparian zone for evapoconcentration effects. This could, for example, be achieved by introducing a concentration correction factor for each sampling day proportional to potential evapotranspiration (PET) or the deviation from the local meteoric water line (LMWL). In our study, the stable water isotope data collected concurrently with the NO_3^- isotope data facilitated the assessment of evaporation effects in riparian groundwater. If stable water isotope data are not available, it might be needed to measure or derive other proxies for evaporation and correct or exclude sampling dates from the modelling that fall within periods of strong evaporation. Similar to the testing of different enrichment factors, the SISS-N model is a convenient tool for running multiple simulations with subsets of the entire data set and thus allows examining the impact of site-specific factors such as evapoconcentration.

6. Conclusions

This paper presents the SISS-N model, which is a simple mathematical model combining isotope and concentration data of NO_3^- to distinguish between denitrification as permanent nitrogen sink and nitrogen retention by other processes (e.g., plant uptake, microbial assimilation, and NO_3^- reduction to ammonium). The model was applied to riparian groundwater wells along a 2-km river reach surrounded by intense agriculture. Based on the model, NO_3^- removal from riparian groundwater via additional processes substantially surpassed denitrification (mean of 26.7% ± 19.0% vs. 11.5% ± 14.9%, respectively, using $\delta^{15}N$ values and $\varepsilon_N = -28.0‰$), especially at further distance from the river and in winter. The rapid decline of denitrification with increasing distance from the river underlines the role of river water as organic carbon source for denitrification. More generally, these results demonstrate that total NO_3^- removal (derived from the concentration reduction relative to a conservative tracer) should not be equated with denitrification, as this might result in significant overestimation of permanent nitrogen removal in riparian zones. This questions the efficacy of relying solely on riparian denitrification to mitigate NO_3^- pollution of rivers, at least for comparable agricultural river sections that are dominated by groundwater flow and dependent on stream water for organic carbon supply.

Overall, this analysis demonstrates the added value of NO_3^- isotope data not only as evidence for denitrification but also for the quantification of denitrification and additional NO_3^- removal processes in riparian groundwater. Moreover, in contrast to previous research on aquifer plumes under steady state conditions, this study is the first application of the SISS model to a diffuse pollutant and time-variant conditions. The extension of the original model to the SISS-N model offers the advantage of assessing apparent NO_3^- removal from riparian groundwater in response not only to dilution and denitrification but also to various biogeochemical processes resulting in N retention in riparian zones. Moreover, the extensive uncertainty analysis indicated a minor impact of various sources of uncertainty, which underlines the validity of the general model outcomes. These results highlight the general capacity of the new SISS-N model to differentiate between denitrification and additional removal processes, while accounting for mixing of groundwater and river water in riparian zones. This allows identifying spatial and temporal patterns of NO_3^- sinks in riparian zones. More generally, we provide a tool for the quantification of permanent NO_3^- removal via denitrification in systems where several transformation and mixing processes co-occur and complicate the assessment of denitrification. The model is thus an important addition to concentration-based end-member mixing models, which provide estimates for total NO_3^- removal solely, as well as to previous studies using field

Acknowledgments
S. R. L. conceived the analyses, performed the computations, and wrote the manuscript; N. T., A. M., and B. M. v. B. contributed to model development and discussion of field data; S. R. L. and A. M. produced the figures, and all authors discussed the results and commented on the manuscript. We thank Toralf Keller, Helko Kotas, Andreas Schoßland, and Oliver Bednorz for carrying out the field work. We would also like to acknowledge Martina Neuber, Sibylle Mothes, Jürgen Steffen, and Kerstin Puschendorf for their laboratory work. The SISS-N model code as well as the chloride and nitrate concentration data, and the nitrate and stable water isotope data are publicly available (doi:10.4211/

isotope data of NO_3^-, which did not account for concentration reduction due to mixing processes and additional NO_3^- sinks in riparian groundwater.

While our model allows distinguishing between denitrification and additional NO_3^- removal processes, we did not attempt to further quantify the potential contribution of each additional process to overall NO_3^- removal. Hence, future research might combine our model with detailed measurement of field parameters that allow quantifying individual removal processes other than denitrification (e.g., by comparing vegetated and non-vegetated sites or different plant communities to elucidate the role of plant uptake). Moreover, model uncertainties can generally arise from limited knowledge of isotope fractionation under field conditions during denitrification and, possibly, additional NO_3^- removal processes. While this is a challenge for every quantification method using field isotope data of NO_3^-, we recommend that future research should focus on the quantification of potential isotope fractionation effects associated with additional uptake and transformation processes in riparian zones such as DNRA and microbial assimilation, as well as on the potential for anammox in riparian groundwater. This would yield more robust denitrification estimates with our model at sites where such processes may be significant. Despite these uncertainties, our model provides a simple method to quantify NO_3^- removal processes over long periods for which continuous measurement of field parameters and reaction products can become impractical. Hence, the SISS-N model has potential for applications at various temporal and spatial scales to obtain a more detailed picture of NO_3^- mixing and transformation processes in riparian zones. This information can ultimately help assess and improve the configuration of riparian zones in order to reduce NO_3^- pollution in catchments.

References

Ahn, C., & Peralta, R. M. (2012). Soil properties are useful to examine denitrification function development in created mitigation wetlands. *Ecological Engineering*, *49*, 130–136. https://doi.org/10.1016/j.ecoleng.2012.08.039

Anderson, T. R., Groffman, P. M., Kaushal, S. S., & Walter, M. T. (2014). Shallow groundwater denitrification in riparian zones of a headwater agricultural landscape. *Journal of Environmental Quality*, *43*, 732–744. https://doi.org/10.2134/jeq2013.07.0303

Bach, M., & Frede, H. G. (1998). Agricultural nitrogen, phosphorus and potassium balances in Germany—Methodology and trends 1970 to 1995. *Z. Pflanzenernähr. Bodenkunde*, *161*, 385–393. https://doi.org/10.1002/jpln.1998.3581610406

Baker, M. A., de Guzman, G., & Ostermiller, J. D. (2009). Differences in nitrate uptake among benthic algal assemblages in a mountain stream. *Journal of the North American Benthological Society*, *28*, 24–33. https://doi.org/10.1899/07-129.1

Barford, C. C., Montoya, J. P., Altabet, M. A., & Mitchell, R. (1999). Steady-State nitrogen isotope effects of N_2 and N_2O production in *Paracoccus denitrificans*. *Applied and Environmental Microbiology*, *65*, 989–994.

Bauersachs, T., Schouten, S., Compaoré, J., Wollenzien, U., Stal, L. J., & Sinninghe Damsteé, J. S. (2009). Nitrogen isotopic fractionation associated with growth on dinitrogen gas and nitrate by cyanobacteria. *Limnology and Oceanography*, *54*, 1403–1411.

Blicher-Mathiesen, G., McCarty, G. W., & Nielsen, L. P. (1998). Denitrification and degassing in groundwater estimated from dissolved dinitrogen and argon. *Journal of Hydrology*, *208*, 16–24. https://doi.org/10.1016/S0022-1694(98)00142-5

Böhlke, J. K., Wanty, R., Tuttle, M., Delin, G., & Landon, M. (2002). Denitrification in the recharge area and discharge area of a transient agricultural nitrate plume in a glacial outwash sand aquifer, Minnesota. *Water Resources Research*, *38*(7), 1105. https://doi.org/10.1029/2001WR000663

Bragan, R. J., Starr, J. L., & Parkin, T. B. (1997). Shallow groundwater denitrification rate measurement by acetylene block. *Journal of Environmental Quality*, *26*, 1531–1538. https://doi.org/10.2134/jeq1997.00472425002600060012x

Burgin, A. J., & Hamilton, S. K. (2007). Have we overemphasized the role of denitrification in aquatic ecosystems? A review of nitrate removal pathways. *Frontiers in Ecology and the Environment*, *5*, 89–96. https://doi.org/10.1890/1540-9295(2007)5[89:HWOTRO]2.0.CO;2

Casciotti, K. L., Sigman, D. M., Hastings, M. G., Böhlke, J. K., & Hilkert, A. (2002). Measurement of the oxygen isotopic composition of nitrate in seawater and freshwater using the denitrifier method. *Analytical Chemistry*, *74*, 4905–4912. https://doi.org/10.1021/ac020113w

Clément, J. C., Holmes, R. M., Peterson, B. J., & Pinay, G. (2003). Isotopic investigation of denitrification in a riparian ecosystem in western France. *Journal of Applied Ecology*, *40*, 1035–1048. https://doi.org/10.1111/j.1365-2664.2003.00854.x

Colman, B. P., Fierer, N., & Schimel, J. P. (2007). Abiotic nitrate incorporation in soil: Is it real? *Biogeochemistry*, *84*, 161–169. https://doi.org/10.1007/s10533-007-9111-5

Coplen, T. B. (2011). Guidelines and recommended terms for expression of stable-isotope-ratio and gas-ratio measurement results. *Rapid Communications in Mass Spectrometry*, *25*, 2538–2560. https://doi.org/10.1002/rcm.5129

Davidson, E. A., Chorover, J., & Dail, D. B. (2003). A mechanism of abiotic immobilization of nitrate in forest ecosystems: The ferrous wheel hypothesis. *Global Change Biology*, *9*, 228–236. https://doi.org/10.1046/j.1365-2486.2003.00592.x

Davis, J. H., Griffith, S. M., Horwath, W. R., Steiner, J. J., & Myrold, D. D. (2008). Denitrification and nitrate consumption in an herbaceous riparian area and perennial ryegrass seed cropping system. *Soil Science Society of America Journal*, *72*(5), 1299–1310. https://doi.org/10.2136/sssaj2007.0279

Denk, T. R. A., Mohn, J., Decock, C., Lewicka-Szczebak, D., Harris, E., Butterbach-Bahl, K., et al. (2017). The nitrogen cycle: A review of isotope effects and isotope modeling approaches. *Soil Biology and Biochemistry*, *105*, 121–137.

Deutsch, B., Mewes, M., Liskow, I., & Voss, M. (2006). Quantification of diffuse nitrate inputs into a small river system using stable isotopes of oxygen and nitrogen in nitrate. *Organic Geochemistry*, *37*, 1333–1342. https://doi.org/10.1016/j.orggeochem.2006.04.012

Dhondt, K., Boeckx, P., Van Cleemput, O., & Hofman, G. (2003). Quantifying nitrate retention processes in a riparian buffer zone using the natural abundance of 15N in NO_3^-. *Rapid Communications in Mass Spectrometry*, *17*, 2597–2604. https://doi.org/10.1002/rcm.1226

Du, R., Peng, Y., Ji, J., Shi, L., Gao, R., & Li, X. (2019). Partial denitrification providing nitrite: Opportunities of extending application for anammox, Environment International, 131, 105001.DWD Climate Data Center (CDC) (2018). Historical monthly station observations (temperature, pressure, precipitation, sunshine duration, etc.) for Germany, version v007. ftp://ftp-cdc.dwd.de/pub/CDC/observations_germany/climate/monthly/kl/historical/, last accessed on 03 May 2019.

Dupas, R., Musolff, A., Jawitz, J. W., Rao, P. S. C., Jäger, C. G., Fleckenstein, J. H., et al. (2017). Carbon and nutrient export regimes from headwater catchments to downstream reaches. *Biogeosciences*, *14*, 4391–4407. https://doi.org/10.5194/bg-14-4391-2017

European Commission (2016). Commission refers Germany to the Court of Justice of the EU over water pollution caused by nitrates. European Commission press release on 28 April 2016, 2016. http://europa.eu/rapid/press-release_IP-16-1453_en.htm, last accessed on 4 May 2018.

European Union (2010): The EU Nitrates Directive. http://ec.europa.eu/environment/pubs/pdf/factsheets/nitrates.pdf, last accessed on 11 January 2019.

Gassen, N., Griebler, C., Werban, U., Trauth, N., & Stumpp, C. (2017). High resolution monitoring above and below the groundwater table uncovers small-scale hydrochemical gradients. *Environmental Science & Technology*, *51*, 13806–13815. https://doi.org/10.1021/acs.est.7b03087

Granger, J., Sigman, D. M., Lehmann, M. F., & Tortell, P. D. (2008). Nitrogen and oxygen isotope fractionation during dissimilatory nitrate reduction by denitrifying bacteria. *Limnology and Oceanography*, *53*, 2533–2545. https://doi.org/10.4319/lo.2008.53.6.2533

Granger, J., & Wankel, S. D. (2016). Isotopic overprinting of nitrification on denitrification as a ubiquitous and unifying feature of environmental nitrogen cycling. *Proceedings of the National Academy of Sciences of the United States of America*, *113*(42), E6391–E6400. https://doi.org/10.1073/pnas.1601383113

Groffman, P. M., Altabet, M. A., Böhlke, J. K., Butterbach-Bahl, K., David, M. B., Firestone, M. K., et al. (2006). Methods for measuring denitrification: Diverse approaches to a difficult problem. *Ecological Applications*, *16*, 2091–2122. https://doi.org/10.1890/1051-0761(2006)016[2091:MFMDDA]2.0.CO;2

Hall, S. J., Weintraub, S. R., & Bowling, D. R. (2016). Scale-dependent linkages between nitrate isotopes and denitrification in surface soils: Implications for isotope measurements and models. *Oecologia*, *181*, 1221–1231. https://doi.org/10.1007/s10533-014-0010-2

Hill, A. R. (1996). Nitrate removal in stream riparian zones. *Journal of Environmental Quality*, *25*, 743–755. https://doi.org/10.2134/jeq1996.00472425002500040014x

Hill, A. R., Devito, K. J., & Vidon, P. G. (2014). Long-term nitrate removal in a stream riparian zone. *Biogeochemistry*, *121*, 425–439. https://doi.org/10.1007/s10533-014-0010-2

Högberg, P., Högberg, M. N., Quist, M. E., Ekblad, A., & Näsholm, T. (1999). Nitrogen isotope fractionation during nitrogen uptake by ectomycorrhizal and non-mycorrhizal Pinus sylvestris. *New Phytologist*, *142*, 569–576. https://doi.org/10.1046/j.1469-8137.1999.00404.x

Hosono, T., Alvarez, K., Lin, I.-T., & Shimada, J. (2015). Nitrogen, carbon, and sulfur isotopic change during heterotrophic (Pseudomonas aureofaciens) and autotrophic (Thiobacillus denitrificans) denitrification reactions. *Journal of Contaminant Hydrology*, *183*, 72–81. https://doi.org/10.1016/j.jconhyd.2015.10.009

Hu, Q., Westerhoff, P., & Vermaas, W. (2000). Removal of nitrate from groundwater by cyanobacteria: Quantitative assessment of factors influencing nitrate uptake. *Applied and Environmental Microbiology*, *66*, 133–139. https://doi.org/10.1128/aem.66.1.133-139.2000

Jahangir, M. M. R., Fenton, O., Müller, C., Harrington, R., Johnston, P., & Richards, K. G. (2017). In situ denitrification and DNRA rates in groundwater beneath an integrated constructed wetland. *Water Research*, *111*, 254–264. https://doi.org/10.1016/j.watres.2017.01.015

Judd, K. E., Likens, G. E., & Groffman, P. M. (2007). High nitrate retention during winter in soils of the Hubbard Brook Experimental Forest. *Ecosystems*, *10*, 217–225. https://doi.org/10.1007/s10021-007-9027-x

Karsh, K. L., Granger, J., Kritee, K., & Sigman, D. M. (2012). Eukaryotic assimilatory nitrate reductase fractionates N and O isotopes with a ratio near unity. *Environmental Science & Technology*, *46*, 5727–5735. https://doi.org/10.1021/es204593q

Kendall, C. (1998). Chapter 16—Tracing nitrogen sources and cycling in catchments. In *Isotope Tracers in Catchment Hydrology*, (pp. 519–576). Amsterdam: Elsevier.

Kendall, C., Elliott, E. M., & Wankel, S. D. (2007). Tracing anthropogenic inputs of nitrogen to ecosystems. In R. Michener & K. Lajtha (Eds.). *Stable Isotopes in Ecology and Environmental Science* (pp. 375–449). Boston: Blackwell Publishing Ltdhttps://doi.org/10.1002/9780470691854.ch12

Kim, K.-H., Yun, S.-T., Mayer, B., Lee, J.-H., Kim, T.-S., & Kim, H.-K. (2015). Quantification of nitrate sources in groundwater using hydrochemical and dual isotopic data combined with a Bayesian mixing model. *Agriculture, Ecosystems & Environment*, *199*, 369–381. https://doi.org/10.1016/j.agee.2014.10.014

Knöller, K., Vogt, C., Haupt, M., Feisthauer, S., & Richnow, H.-H. (2011). Experimental investigation of nitrogen and oxygen isotope fractionation in nitrate and nitrite during denitrification. *Biogeochemistry*, *103*, 371–384. https://doi.org/10.1007/s10533-010-9483-9

Lambert, T., Pierson-Wickmann, A.-C., Gruau, G., Thibault, J.-N., & Jaffrezic, A. (2011). Carbon isotopes as tracers of dissolved organic carbon sources and water pathways in headwater catchments. *Journal of Hydrology*, *402*, 228–238.

Landwehr, J. M., & Coplen, T. B. (2006). Line-conditioned excess: A new method for characterizing stable hydrogen and oxygen isotope ratios in hydrologic systems. In *International Conference on Isotopes in Environmental Studies*, (pp. 132–135). Vienna: IAEA.

Li, X., Rennenberg, H., & Simon, J. (2016). Seasonal variation in N uptake strategies in the understorey of a beech-dominated N-limited forest ecosystem depends on N source and species. *Tree Physiology*, *36*, 589–600. https://doi.org/10.1093/treephys/tpv132

Lund, L. J., Horne, A. J., & Williams, A. E. (1999). Estimating denitrification in a large constructed wetland using stable nitrogen isotope ratios. *Ecological Engineering*, *14*, 67–76. https://doi.org/10.1016/S0925-8574(99)00020-8

Lutz, S. R., & Van Breukelen, B. M. (2014a). Combined source apportionment and degradation quantification of organic pollutants with CSIA: 1. Model Derivation. *Environmental Science & Technology*, *48*, 6220–6228. https://doi.org/10.1021/es405400w

Lutz, S. R., & Van Breukelen, B. M. (2014b). Combined source apportionment and degradation quantification of organic pollutants with CSIA: 2. Model validation and application. *Environmental Science & Technology*, *48*, 6229–6236. https://doi.org/10.1021/es4054016

Mariotti, A., Germon, J. C., Hubert, P., Kaiser, P., Letolle, R., Tardieux, A., & Tardieux, P. (1981). Experimental determination of nitrogen kinetic isotope fractionation: Some principles; illustration for the denitrification and nitrification processes. *Plant and Soil*, *62*, 413–430. https://doi.org/10.1007/bf02374138

Mariotti, A., Mariotti, F., Champigny, M.-L., Amarger, N., & Moyse, A. (1982). Nitrogen isotope fractionation associated with nitrate reductase activity and uptake of NO3− by pearl millet. *Plant Physiology*, *69*, 880–884. https://doi.org/10.1104/pp.69.4.880,1982

Matheson, F. E., Nguyen, M. L., Cooper, A. B., Burt, T. P., & Bull, D. C. (2002). Fate of ^{15}N-nitrate in unplanted, planted and harvested riparian wetland soil microcosms. *Ecological Engineering*, *19*, 249–264. https://doi.org/10.1016/S0925-8574(02)00093-9

Matiatos, I. (2016). Nitrate source identification in groundwater of multiple land-use areas by combining isotopes and multivariate statistical analysis: A case study of Asopos basin (Central Greece). *Science of The Total Environment*, *541*, 802–814. https://doi.org/10.1016/j.scitotenv.2015.09.134

Mayer, P. M., Reynolds, S. K., McCutchen, M. D., & Canfield, T. J. (2007). Meta-analysis of nitrogen removal in riparian buffers. *Journal of Environmental Quality*, *36*, 1172–1180. https://doi.org/10.2134/jeq2006.0462

McCarty, G. W., Mookherji, S., & Angier, J. T. (2007). Characterization of denitrification activity in zones of groundwater exfiltration within a riparian wetland ecosystem. *Biology and Fertility of Soils*, *43*, 691–698. https://doi.org/10.1007/s00374-006-0151-0

McPhillips, L. E., Groffman, P. M., Goodale, C. L., & Walter, M. T. (2015). Hydrologic and biogeochemical drivers of riparian denitrification in an agricultural watershed. *Water, Air, & Soil Pollution*, *226*, 169. https://doi.org/10.1007/s11270-015-2434-2

Mengis, M., Schif, S. L., Harris, M., English, M. C., Aravena, R., Elgood, R., & MacLean, A. (1999). Multiple geochemical and isotopic approaches for assessing ground water NO_3^- elimination in a riparian zone. *Groundwater*, *37*, 448–457. https://doi.org/10.1111/j.1745-6584.1999.tb01124.x

Muñoz, N., Guerri, J., Legaz, F., & Primo-millo, E. (1993). Seasonal uptake of 15N-nitrate and distribution of absorbed nitrogen in peach trees. *Plant and Soil*, *150*, 263–269. https://doi.org/10.1007/bf00013023

Naeher, S., Huguet, A., Roose-Amsaleg, C. L., Laverman, A. M., Fosse, C., Lehmann, M. F., et al. (2015). Molecular and geochemical constraints on anaerobic ammonium oxidation (anammox) in a riparian zone of the Seine Estuary (France). *Biogeochemistry*, *123*, 237–250. https://doi.org/10.1007/s10533-014-0066-z

Nikolenko, O., Jurado, A., Borges, A. V., Knöller, K., & Brouyère, S. (2018). Isotopic composition of nitrogen species in groundwater under agricultural areas: A review. *Science of The Total Environment*, *621*, 1415–1432. https://doi.org/10.1016/j.scitotenv.2017.10.086

Nixdorf, E., & Trauth, N. (2018). Evaluating the reliability of time series analysis to estimate variable riparian travel times by numerical groundwater modelling. *Hydrological Processes*, *32*, 408–420. https://doi.org/10.1002/hyp.11428

Ong, C. G., Tanji, K. K., Dahlgren, R. A., Smith, G. R., & Quek, A. F. (1995). Water quality and trace element evapoconcentration in evaporation ponds for agricultural waste water disposal. *Journal of Agricultural and Food Chemistry*, *43*, 1941–1947. https://doi.org/10.1021/jf00055a034

Osborne, L. L., & Kovacic, D. A. (1993). Riparian vegetated buffer strips in water-quality restoration and stream management. *Freshwater Biology*, *29*, 243–258. https://doi.org/10.1111/j.1365-2427.1993.tb00761.x

Otero, N., Torrentó, C., Soler, A., Menció, A., & Mas-Pla, J. (2009). Monitoring groundwater nitrate attenuation in a regional system coupling hydrogeology with multi-isotopic methods: The case of Plana de Vic (Osona, Spain). *Agriculture, Ecosystems & Environment*, *133*, 103–113. https://doi.org/10.1016/j.agee.2009.05.007

Pfenning, K. S., & McMahon, P. B. (1997). Effect of nitrate, organic carbon, and temperature on potential denitrification rates in nitrate-rich riverbed sediments. *Journal of Hydrology*, *187*, 283–295. https://doi.org/10.1016/S0022-1694(96)03052-1

Providoli, I., Bugmann, H., Siegwolf, R., Buchmann, N., & Schleppi, P. (2006). Pathways and dynamics of $^{15}NO_3^-$ and $^{15}NH_4^+$ applied in a mountain Picea abies forest and in a nearby meadow in central Switzerland. *Soil Biology and Biochemistry*, *38*, 1645–1657. https://doi.org/10.1016/j.soilbio.2005.11.019

Rivett, M. O., Buss, S. R., Morgan, P., Smith, J. W. N., & Bemment, C. D. (2008). Nitrate attenuation in groundwater: A review of biogeochemical controlling processes. *Water Research*, *42*, 4215–4232. https://doi.org/10.1016/j.watres.2008.07.020

Rode, M., Halbedel Née Angelstein, S., Anis, M. R., Borchardt, D., & Weitere, M. (2016). Continuous in-stream assimilatory nitrate uptake from high-frequency sensor measurements. *Environmental Science & Technology*, *50*, 5685–5694. https://doi.org/10.1021/acs.est.6b00943

Saunders, D. L., & Kalff, J. (2001). Denitrification rates in the sediments of Lake Memphremagog, Canada–USA. *Water Research*, *35*, 1897–1904. https://doi.org/10.1016/S0043-1354(00)00479-6

Schilling, K. E., Kult, K., Wilke, K., Streeter, M., & Vogelgesang, J. (2017). Nitrate reduction in a reconstructed floodplain oxbow fed by tile drainage. *Ecological Engineering*, *102*, 98–107. https://doi.org/10.1016/j.ecoleng.2017.02.006

Seibert, J., Grabs, T., Köhler, S., Laudon, H., Winterdahl, M., & Bishop, K. (2009). Linking soil- and stream-water chemistry based on a Riparian Flow-Concentration Integration Model. *Hydrology and earth system sciences*, *13*, 2287–2297. https://doi.org/10.5194/hess-13-2287-2009

Seitzinger, S. P. (1994). Linkages between organic matter mineralization and denitrification in eight riparian wetlands. *Biogeochemistry*, *25*, 19–39. https://doi.org/10.1007/bf00000510

Seitzinger, S. P., Styles, R. V., Boyer, E. W., Alexander, R. B., Billen, G., Howarth, R. W., et al. (2002). Nitrogen retention in rivers: model development and application to watersheds in the northeastern U.S.A. *Biogeochemistry*, *57*, 199–237. https://doi.org/10.1023/a:1015745629794

Shang, P., Lu, Y., Du, Y., Jaffé, R., Findlay, R. H., & Wynn, A. (2018). Climatic and watershed controls of dissolved organic matter variation in streams across a gradient of agricultural land use. *Science of The Total Environment*, *612*, 1442–1453.

Sigman, D. M., Casciotti, K. L., Andreani, M., Barford, C., Galanter, M., & Böhlke, J. K. (2001). A bacterial method for the nitrogen isotopic analysis of nitrate in seawater and freshwater. *Analytical Chemistry*, *73*, 4145–4153. https://doi.org/10.1021/ac010088e

Stanford, G., Dzienia, S., & Vander Pol, R. A. (1975). Effect of temperature on denitrification rate in soils. *Soil Science Society of America Journal*, *39*, 867–870. https://doi.org/10.2136/sssaj1975.03615995003900050024x

Sutka, R. L., Ostrom, N. E., Ostrom, P. H., Breznak, J. A., Gandhi, H., Pitt, A. J., & Li, F. (2006). Distinguishing nitrous oxide production from nitrification and denitrification on the basis of isotopomer abundances. *Applied and Environmental Microbiology*, *72*, 638–644. https://doi.org/10.1128/aem.72.1.638-644.2006

Torrentó, C., Cama, J., Urmeneta, J., Otero, N., & Soler, A. (2010). Denitrification of groundwater with pyrite and *Thiobacillus denitrificans*. *Chemical Geology*, *278*, 80–91. https://doi.org/10.1016/j.chemgeo.2010.09.003

Torrentó, C., Urmeneta, J., Otero, N., Soler, A., Viñas, M., & Cama, J. (2011). Enhanced denitrification in groundwater and sediments from a nitrate-contaminated aquifer after addition of pyrite. *Chemical Geology*, *287*, 90–101. https://doi.org/10.1016/j.chemgeo.2011.06.002

Trauth, N., & Fleckenstein, J. H. (2017). Single discharge events increase reactive efficiency of the hyporheic zone. *Water Resources Research*, *53*, 779–798. https://doi.org/10.1002/2016WR019488

Trauth, N., Musolff, A., Knöller, K., Kaden, U. S., Keller, T., Werban, U., & Fleckenstein, J. H. (2018). River water infiltration enhances denitrification efficiency in riparian groundwater. *Water Research*, *130*, 185–199. https://doi.org/10.1016/j.watres.2017.11.058

Trauth, N., Schmidt, C., Vieweg, M., Oswald, S. E., & Fleckenstein, J. H. (2015). Hydraulic controls of in-stream gravel bar hyporheic exchange and reactions. *Water Resources Research*, *51*, 2243–2263. https://doi.org/10.1002/2014WR015857

Treibergs, L. A., & Granger, J. (2017). Enzyme level N and O isotope effects of assimilatory and dissimilatory nitrate reduction. *Limnology and Oceanography*, *62*, 272–288. https://doi.org/10.1002/lno.10393

Vidon, P. G. F., & Hill, A. R. (2004). Landscape controls on nitrate removal in stream riparian zones. *Water Resources Research*, *40*, W03201. https://doi.org/10.1029/2003WR002473

Vought, L. B.-M., Dahl, J., Pedersen, C. L., & Lacoursière, J. O. (1994). Nutrient retention in riparian ecotones. *Ambio*, *23*, 342–348. www.jstor.org/stable/431423

Wang, M., Lu, B., Wang, J., Zhang, H., Guo, L., & Lin, H. (2016). Using dual isotopes and a bayesian isotope mixing model to evaluate nitrate sources of surface water in a drinking water source watershed, East China. *Water*, *8*, 355. https://doi.org/10.3390/w8080355

Wang, S.,Zhu, G., Zhuang, L., Li, Y., Liu, L., Lavik, G., et al. (2020). Anaerobic ammonium oxidation is a major N-sink in aquifer systems around the world. *ISME Journal*, *14*, 151–163. https://doi.org/10.1038/s41396-019-0513-x

Wellman, R. P., Cook, F. D., & Krouse, H. R. (1968). Nitrogen-15: Microbiological alteration of abundance. *Science*, *161*, 269–270. https://doi.org/10.1126/science.161.3838.269

Wexler, S. K., Goodale, C. L., McGuire, K. J., Bailey, S. W., & Groffman, P. M. (2014). Isotopic signals of summer denitrification in a northern hardwood forested catchment. *Proceedings of the National Academy of Sciences*, *111*, 16413–16418. https://doi.org/10.1073/pnas.1404321111

Wollschläger, U., Attinger, S., Borchardt, D., Brauns, M., Cuntz, M., Dietrich, P., et al. (2016). The Bode hydrological observatory: A platform for integrated, interdisciplinary hydro-ecological research within the TERENO Harz/Central German Lowland Observatory. *Environmental Earth Sciences*, *76*, 29. https://doi.org/10.1007/s12665-016-6327-5

Wunderlich, A., Meckenstock, R., & Einsiedl, F. (2012). Effect of different carbon substrates on nitrate stable isotope fractionation during microbial denitrification. *Environmental Science & Technology*, *46*, 4861–4868. https://doi.org/10.1021/es204075b

Xue, D., Botte, J., De Baets, B., Accoe, F., Nestler, A., Taylor, P., et al. (2009). Present limitations and future prospects of stable isotope methods for nitrate source identification in surface- and groundwater. *Water Research*, *43*, 1159–1170. https://doi.org/10.1016/j.watres.2008.12.048

Yoneyama, T., Matsumaru, T., Usui, K., & Engelaar, W. M. H. G. (2001). Discrimination of nitrogen isotopes during absorption of ammonium and nitrate at different nitrogen concentrations by rice (Oryza sativa L.) plants. *Plant, Cell & Environment*, *24*, 133–139. https://doi.org/10.1046/j.1365-3040.2001.00663.x

Zacharias, S., Bogena, H., Samaniego, L., Mauder, M., Fuß, R., Pütz, T., et al. (2011). A network of terrestrial environmental observatories in Germany. *Vadose Zone Journal*, *10*, 955–973. https://doi.org/10.2136/vzj2010.0139

Zhi, W., Li, L., Dong, W., Brown, W., Kaye, J., Steefel, C., & Williams, K. H. (2019). Distinct source water chemistry shapes contrasting concentration-discharge patterns. *Water Resources Research*, *55*, 4233–4251. https://doi.org/10.1029/2018WR024257